On Organic Liquid Crystal Transfer from Bitumen-Rich to Water-Rich Phases: A Combined Laboratory and SAGD Field Study

by

Chuan Qin

A thesis submitted to the Faculty of Graduate Studies and Research

in partial fulfillment of the requirements for the degree of

Master of Science

in

Chemical Engineering

Chemical and Materials Engineering

Spring 2014

Edmonton, Alberta

Abstract

Hydrocarbon-based liquid-crystal domains were observed in unreacted heavy fractions extracted from Athabasca bitumen and bitumen derived hydrocarbon resource fractions. Transfer of these organic crystalline domains to the water-rich phase during SAGD production is explored here because there removal, required for optimal operation of boilers used for water recycling, is unlike the removal of oil drops and dissolved oil from the water phase and their fate in water recycling processes is unknown. In this work, a fraction of these liquid-crystal rich domains present initially in bitumen are shown to be transferred to the water-rich phase in both laboratory experiments and industrial SAGD production facilities and possible transfer mechanisms are discussed. Tracing the fate of the liquid crystal domains in SAGD surface facilities revealed that SAGD water treatment processes eliminate liquid crystals from the water rich phase, during normal operation, as liquid crystals were not detected in the feed stream to the steam generator. The roles played by chemical additives, and their presence, comprise uncontrolled variables in the field study. Future work will focus on the individual unit operations of the water de-oiling and treatment process at a single facility to determine where and how the liquid crystals are eliminated from the produced water during normal operation. An approach for preparing liquid-crystal enriched samples is also proposed.

Acknowledgement

A thesis almost always arises from collaboration, even if it has only a single author appears on the front page. First and foremost, I would give my sincere gratitude to my supervisor Dr. John Shaw. Life is all about the people you meet, and it is my great fortune to have you during my study years in Canada. This is not only for the enthusiastic supervision, remarkable tolerance and patience, fully trust and support you given which drive me to overcome the obstacles continuously and complete this project, but also for the opportunities you provided, the life lessons you taught which help me keep growing and affect the way I see the world in some profoundly way. And I will always be grateful and keep these in mind as I am stepping into the next stage of my career.

I was also lucky enough to be surrounded by all the warm colleagues from the petroleum thermodynamic group in the past two years; their smiles and kind assistance ran throughout my research life here. I would like to thank Dr. Reza Bagheri and Mr. Brady Masik for the equipment training and discussions at the initial stage of my project; I also thank Ms. Mildred Becerra for technical assistance in the lab, Dr. Ala bazyleva for reviewing the thesis and giving critical comments and Ms. Linda Kaert for assisting me with travel expense claims and other financial issues.

The support from external collaborators was also indispensable for this accomplishment. I thank Mr. Nestor Zerpa (Nexen Inc.), Dr. Yishu Song (ConocoPhillips), Mr. Iboja Tot (Shell) and Dr. Václav Laštovka (Shell) for providing the samples for analysis and discussions regarding technical questions. Great appreciation also goes for all the external sponsors for their stable financial support.

Last but not least, my gratitude goes to my dearest parents, for their whole-hearted support and endless love throughout every stage in my life.

Table of Contents

List of Figures

List of Tables

Nomenclature

FT-ICR	Fourier Transform Ion Cyclotron Resonance
CHWE	Clark Hot Water Extraction
SAGD	Steam Assisted Gravity Drainage
CSS	Cyclical Steam Simulation
BFW	Boiler Feed Water
FWKO	Free Water Knock Out
IGF	Induced Gas Flotation
ORF	Oil Removal Filters
HLS	Hot Lime Softening
WLS	Warm Lime Softening
WAC	Weak Acid Cation
OTSG	Once Through Steam Generator
PSV	Primary Separation Vessel
SARA	Saturate, Aromatic, Resin and Asphaltene
AB	Athabasca Bitumen
PLM	Polarized Light Microscope
TDS	Total Dissolved Solids
XPS	X-ray Photoelectron Spectroscopy
V_{rad}	Outward radial flow velocity
j	Evaporation mass flux
ρ	Density of drop liquid

V_{Ma} Marangoni recirculation flow velocity

ϕ Wetting angle of the drop

μ Dynamic viscosity

β Gradient of surface tension with respect to the temperature

ΔT Temperature difference between the edge and the apex of the droplet

C_R Dimensionless number for quantifying the successful coffee ring formation

τ_{particle} Time that allows the adjacent particles to meet each other at the rim area

τ_{evap} Evaporation time of the droplet

K Parameter representing the droplet evaporation rate

D Diameter of the droplet

$\theta_{initial}$ Initial contact angle

$\theta_{receding}$ Receding contact angle

V_d Volume of the droplet

n The number of dispersed particles in the droplet

D_p Diffusion constant of the particle in a low viscosity liquid medium

Chapter 1 Introduction

1.1 What are Liquid Crystals?

1.1.1 General Definition of Liquid Crystals

The liquid crystal state is an intermediate state between the rigid crystalline solid state, possessing long-range order in three dimensions, and the liquid state, that does not possess long-range order. In this state matter possesses structure or order in one or two dimensions only and thus possesses some solid-like optical properties and some liquid-like flow properties. At the molecular scale, the molecules have orientational order but their translational order is lost [1]. Conventional liquid crystals are typically needle-like or disk-like. Plastic crystals, which are also an intermediate state between isotropic liquid and solid, consist of almost spherical objects [2]. Possible paths linking solid and liquid states are shown in Figure 1-1. The unique physical properties of liquid crystals such as optical anisotropy and electric field sensitivity are widely studied and are the basis on numerous applications in the materials industry [1].

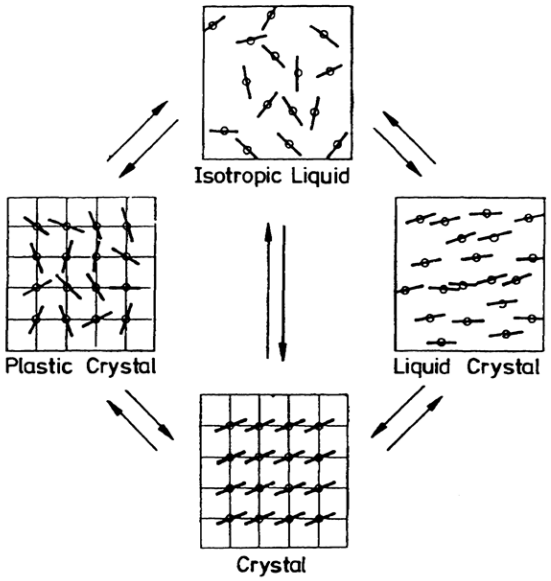

Figure 1-1 Schematic representation of possible transitions between the crystal state and the isotropic liquid state [2].

1.1.2 Types of Liquid Crystals

Compounds, which exhibit liquid crystalline properties in a certain range of temperature and transition to isotropic liquids at higher temperatures, are called thermotropic liquid crystals. Most liquid crystals are thermotropic. Compounds that become liquid crystals on addition of solvents at fixed temperature are called lyotropic liquid crystals. Compounds that exhibit both thermotropic and lyotropic liquid crystal behavior are called amphotropic liquid crystals [3]. The nature of the liquid crystals formed is determined by the local molecular structure order. There are three common classifications: 1) nematic liquid crystals, where molecules have no positional order but tend to align in the same direction; 2) sematic liquid crystals, where the molecules tend to align in layers or planes, showing a degree of translational order that does not exist in the nematic liquid crystals; 3) columnar liquid crystals, where the molecules assemble in two dimensional lattices and the lattices pack together forming discotic columns [4, 5].

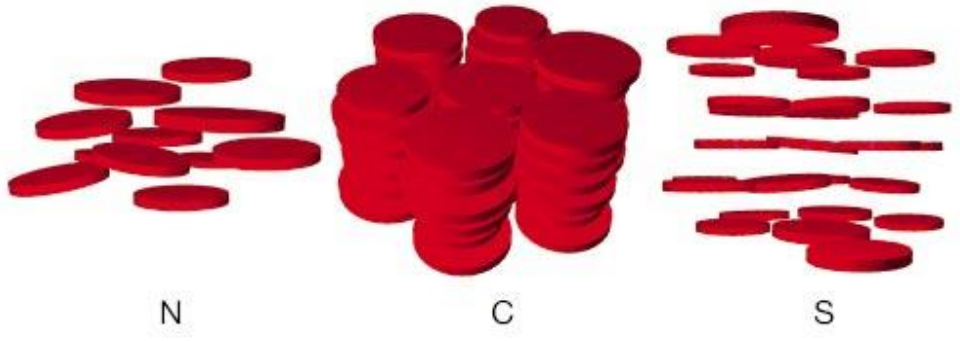

Figure 1-2 Structure of the three main classes of liquid crystals: the nematic phase (N), the columnar phase (C), and the sematic phase (S) [6]

1.2 Liquid Crystals in Unreacted Bitumen and Heavy Oil Resource Fractions

1.2.1 Physical Properties

Liquid crystals were observed in different unreacted petroleum fractions such as Safaniya heptane asphaltenes, Athabasca, Maya and Cold Lake pentane asphaltenes [7]. They all exhibit thermotropic liquid crystalline behavior with varying phase transition temperatures. The liquid crystal forming temperatures are 338 K for Athabasca C_5 asphaltenes, 340 K for Maya C_5 asphaltenes, 341 K for Cold Lake C_5 asphaltenes and 371 K for Safaniya C_7

asphaltenes. The disappearance temperatures are 423 K for Athabasca C_5 asphaltenes, 435 K for Maya C_5 asphaltenes, 431 K for Cold lake C_5 asphaltenes and 433 K for Safaniya C_7 asphaltenes. Upon exposure to toluene vapour, liquid crystals also appear then disappear in the unreacted asphaltenes at fixed temperature. Consequently, the liquid crystals in unreacted bitumen fractions are amphotropic [8] and the liquid crystal type remains unknown.

1.2.2 Composition of Liquid Crystals in Bitumen

Bitumen is a complex ill-defined mixture comprising thousands of compounds and it is challenging to isolate liquid crystal forming fractions even under conditions where they appear. One approach is to collect physically enriched samples and to analyze their compositions [9]. In this approach, C_5 Athabasca asphaltene was first placed on a glass slide and heated to 145°C for one hour. After it was cooled to room temperature, the glass slide together with the C_5 asphaltenes were immersed in a mixture of heptane 90 vol. % + toluene 10 vol. % for 30 minutes. Then the solution containing dissolved liquid crystalline material was evaporated at 95°C. Finally, around 0.5 mg of a solid film attached to the wall of a beaker was collected. This material, defined as a liquid crystal enriched sample, was subject to further analysis.

Figure 1-3 shows the FT-ICR mass spectrum of the liquid crystal enriched sample. Peaks are relatively abundant in the range $200 < m/z < 500$. Such a low and narrow molecular mass range means the liquid crystal material comes from the relatively light portion of the parent asphaltene. The top 17 most abundant heteroatom classes are shown in Figure 1-4. Compared to the heteroatom distribution of Athabasca C_7 asphaltenes, Figure 1-5, the enriched sample derived from the Athabasca C_5 asphaltenes appears to have a higher relative abundances of sulfur, oxygen and nitrogen than the parent C_7 asphaltenes [9]. While these analysis results are suggestive, they are not definitive as FT-ICR-MS results are not fully quantitative.

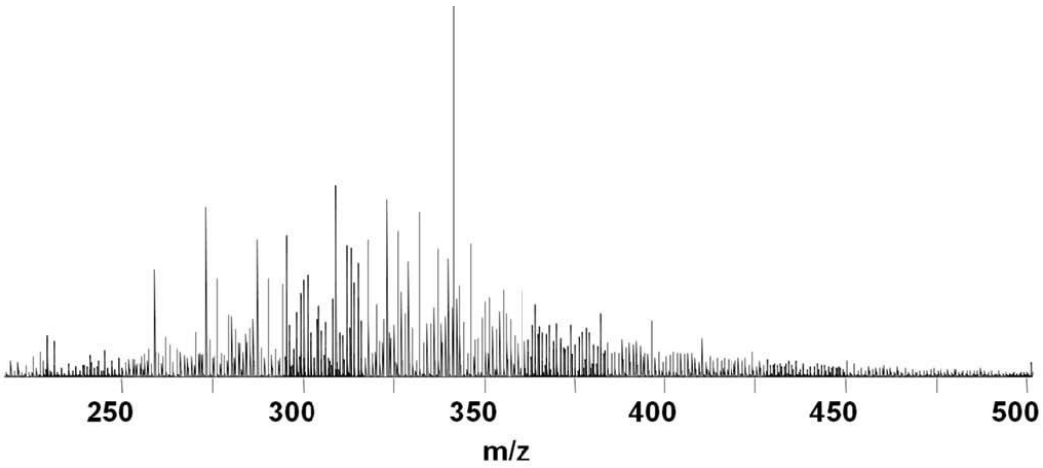

Figure 1-3 Mass spectrum of a liquid crystal enriched sample [9]

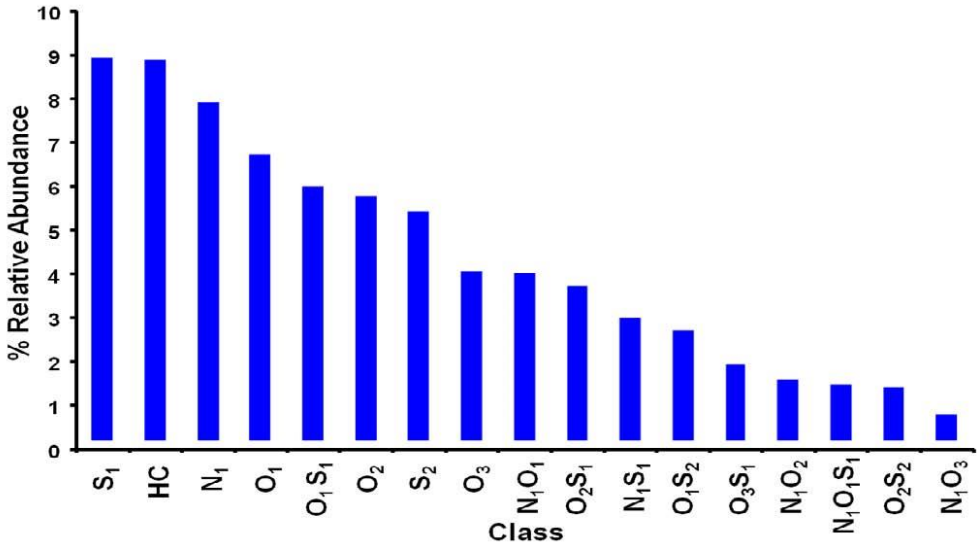

Figure 1-4 Heteroatom abundance distribution for a liquid crystal enriched Athabasca asphaltene derived sample [9]

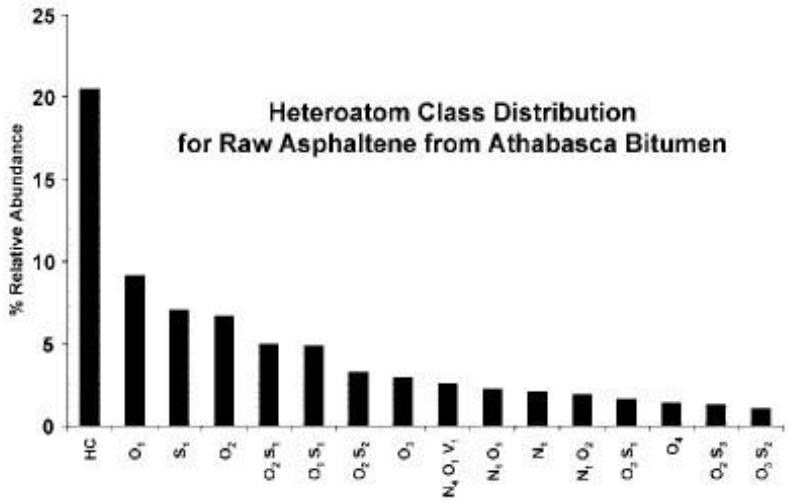

Figure 1-5 Heteroatom abundance distribution for Athabasca C_7 asphaltenes [10]

1.2.3 Liquid Crystals in Bitumen and Heavy Oil Production and Transport

This class of materials was first reported in 2010 and it has not been observed and is not accounted for in conventional resource and resource fraction assays. From an industrial perspective, it comprises an unknown and uncontrolled class of materials potentially present in production and transport processes. The fate of materials comprising this class, processing problems or potential benefits associated with them, are also unknown. From laboratory experiments performed to date [8], the liquid crystal domains comprise ~ 5 to 50 µm diameter spheres, with an outer shell of liquid crystalline material surrounding an isotropic core. These domains are also known to be surface active. Their potential to affect transport phenomena in these multiphase environments is unknown. As Athabasca bitumen is a key Canadian resource, production and surface separation processes for bitumen are reviewed from the perspective of potential impacts of liquid crystals.

1.3 Bitumen Mining and Water Treatment Processes

1.3.1 Surface Mining and Water Extraction Processes

Oil sand normally consists of 7~13 wt. % bitumen, 3~7 wt. % water and 80~85 wt. % mineral solids including clays, fines and sand. Although only 18 % of the Alberta oil sands are buried less than 50 meters under ground, which are mineable by open-pit surface mining, surface mining plays a major role in the Canadian oil sand industry. The Clark Hot Water Extraction (CHWE) process and its modern variants are the primary extraction

methods used to separate oil from oil sand. Several steps are involved in a commercial surface mining operation. The overburden is removed, then the oil baring sand is mined using large scale shovels and trucks. The sand ore lumps are crushed and mixed with hot water to form a slurry and the slurry is pumped through a pipeline to an extraction plant. During transport, the sand, water and bitumen begin to separate. At the plant the slurry is separated into primary bitumen froth, middlings and tailing streams. The bitumen froth (normally containing 60 wt. % bitumen, 30 wt. % water and 10 wt. % fine solids) is treated using naphtha or other paraffinic diluents to remove water and inorganic solids. The bitumen is sent to a refinery unit to be upgraded into light synthetic crude. The water and solids streams are treated further and then disposed of. A simplified process schematic is shown in Figure 1-6 [11].

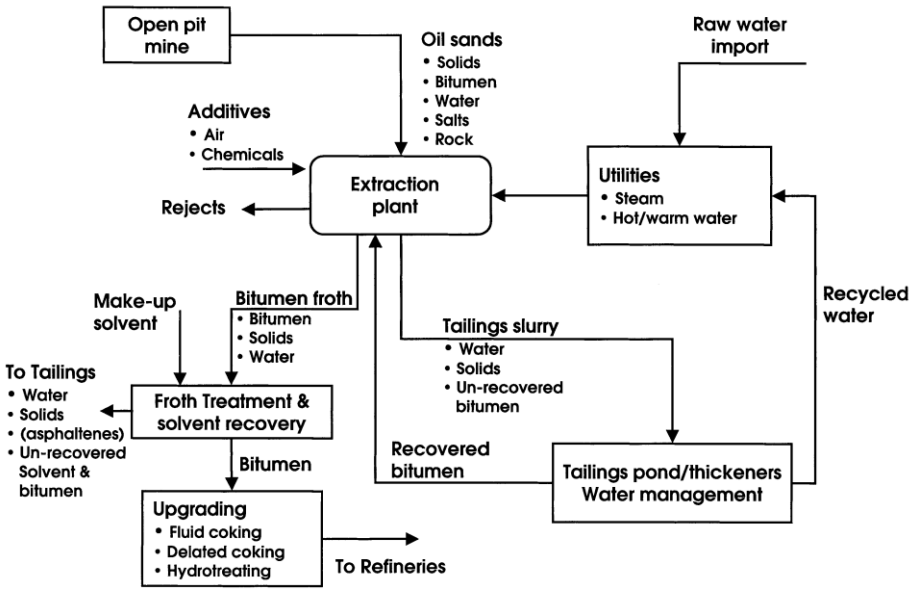

Figure 1-6 Generalized scheme for oil sands processing using water-based extraction technology [11]

1.3.2 Froth Treatment

The stability of water-in-oil emulsions is detrimental in water-based extraction of crude oil from oil sands. During the separation process, the majority of water is easily removed while a significant amount remains dispersed in the hydrocarbon and forms a water-in-oil emulsion. The presence of this undesirable water raises challenges in the dewatering process. During froth treatment, up to 2% water, in the form of extremely stable drops with diameters of 5 μm or less is present in the diluted bitumen froth [12].

The difficulties of identifying the material at the water/oil interface as well as determining their role in emulsion stabilization have been hotly debated. Asphaltenes were first considered as one of the main stabilizing agents in the water/oil interface [12]. However, recently studies are challenging this paradigm. The asphaltene molecular model structures, either island model or archipelago model, show no hydrophilic heads as surfactant molecules do, and the asphaltene molecules consist mostly of hydrophobic fragments so they do not have the amphiphilic character of surfactants [13]. A recent study showed that only a small sub-fraction of asphaltenes (less than 2%) can be involved in water-in-oil emulsion stabilization [14]. Under certain conditions, the material at the interface between the oil and water forms a mesomorphic phase, known as liquid crystals. The phase is organized into a multilayer structure that provides steric stabilization to the water in hydrocarbon interfaces [15]. It was found in these works that liquid crystals are a small fraction of the parent asphaltenes. Further compositional analysis of the oil/water interfacial material from both high-and low-bitumen concentration emulsions was reported [16]. This material, like the liquid crystals identified in bitumen [7], is rich in heteroatom species, but further study is needed to elaborate the link between these two materials. A series of works based on the model mixture sodium naphthenate-water-toluene has been published recently [17, 18]. Thick, viscous liquid crystalline layers of sodium naphthenate at the oil/water interface were observed. However, such a lamellar phase is unlikely to arise under industrial conditions.

1.3.3 Modeling Rag Layers

In froth treatment, centrifugation is typically applied for naphtha diluted froths, while gravity settling is applied to paraffin diluted froths in order to achieve separation. For both cases, rag layers, which are complex mixtures of flocculated water droplets, multiple phase emulsions and relatively fine solids are formed at the water/oil interface in process vessels. Their presence complicates dewatering efficiency. Czarneki and Moran [19] prepared model rag layers that were collected under laboratory conditions based on multi-stage centrifugation. The results indicate optical anisotropy of the materials at drop surfaces that resemble liquid crystal-like behavior, shown in Figure 1-7.

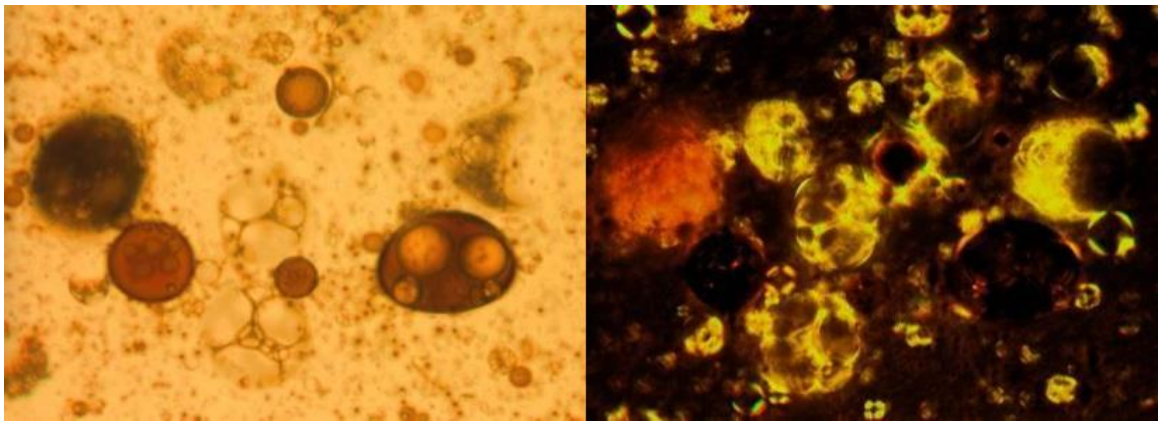

Figure 1-7 Microscopic images of a multiple emulsion in water-diluted bitumen system—left: normal illumination; right: between crossed polarizers [19]**.**

1.4 In-situ Production Processes

1.4.1 Process Overview

Surface mining is not applicable for bitumen deposits that are buried deeper than 75 meters. However, these deposits make up 80 % of the total recoverable bitumen resources in the Athabasca region [20]. In order to recover this portion of the deposits, other recovery processes have been introduced, which are known as the in-situ methods. Two main types of in-situ oil sand extraction are: Steam Assisted Gravity Drainage (SAGD) and Cyclical Steam Simulation (CSS). These technologies usually involve steam injection through vertical or horizontal wells to heat the bitumen deposit so that bitumen can be pumped to the surface for upgrading or refining.

Cyclical Steam Simulation (CSS), also known as “huff and puff”, is a mature technology. This process requires only one wellbore and three stages comprise a production cycle: steam injection, reservoir soaking and bitumen production. During the first stage, steam is injected into the reservoir though the vertical well bore, then the steam is left in the reservoir for several weeks in order to mobilize cold bitumen underground, and finally the emulsion of condensed water and heated bitumen is pumped to the surface through the injection well. After one cycle, the steam is re-injected to start a new cycle after the oil production rate falls below a critical threshold. The periods of injection and production alternate. The Cyclic Steam Simulation is good for deep but thin reservoirs and is currently

used at the Imperial Oil Cold Lake project and at the CNRL Wolf Lake-Primrose project in the North Alberta [21-23].

The Steam Assisted Gravity Drainage (SAGD) process differs from the CSS process in which only a single wellbore is involved, as it comprises parallel pairs of horizontal wells drilled from a central well pad; one is about a few meters above the other. The upper one is known as the injector, while the bottom one is the producer. The process works by injecting steam into the injector well continuously and the steam heats the bitumen, decreases its viscosity enough to flow into the producer well below by gravity. The emulsions of the bitumen, steam condensate and produced water as well as possible gases are piped from the producer well to the surface facility, where they are separated and further treated. Unlike the CSS, the steam injection and oil production happen in different wells and the SAGD process operates continuously and simultaneously [24].

1.4.2 Surface Water Treatment for *in-situ* Production Processes

Both the SAGD and CSS methods require large volumes of water to generate steam for bitumen recovery. The estimated consumption of water is around 1.8~3.0 tonnes steam/m^3 oil for SAGD and 0.3~3.0 tonnes steam/m^3 oil for CSS[25]. Most of water used in these processes is from brackish aquifers rather than from surface sources. Recycling of produced water to generate new steam in the plant is necessity not only because of water supply limitations but also due to restrictions on water disposal. Around 85%~95% of SAGD of produced water is treated and recycled. Certain water quality requirements must be met before produced water can be used as boiler feed water (BFW). Table 1-1 lists the basic quality parameters and their typical requirements for boiler feed water.

Table 1-1 Critical parameter of boiler feed water

Feed Water Quality Parameter	Typical Limits
Dissolved Hardness	Less than 1ppm as $CaCO_3$
Oil (Total Petroleum Hydrocarbons)	Less than 5 ppm
Silica	Less than 50~75 ppm
Dissolved Oxygen	Less than 5 ppb
Conductivity	Less than about 13 mS/cm
Total Dissolved Solid	Less than 8000~10000 ppm

To meet these water quality requirements, different stages of the water treatment are typically applied with the aim to convert as much produced water as possible to recyclable boiler feed water. This dramatically reduces make-up fresh water usage and offers lower total capital and operating costs. Three stages are typically used in surface SAGD water treatment facilities. In the first stage, known as de-oiling, water is separated from produced bitumen. This process can also be divided into preliminary separation and secondary separation. In the second stage, known as the water treatment process, produced water is further treated to remove impurities. In the third stage, it is recycled back to a steam generator for re-injection. However, the details of processes present at individual SAGD plants differ. Three such facilities are described here. All are operating and are located in Northern Alberta. All three plants provided produced water samples for analysis in this work.

1.4.2.1 Shell Orion SAGD Facility Case

Figure 1-8 shows the flow diagram of the Shell Orion SAGD produced water treatment process. Diluent and chemicals are injected into the feed ahead of the primary separator to break the emulsion and to meet the sales oil blending specifications at the outlet. The effluent then flows into a Free-Water-Knock-Out (FWKO) drum followed by an electrostatic grid treater designed to remove residual water drops from the oil phase. The water phase flows to a skim tank to maximize the retention time before it enters the secondary separation stage. The secondary de-oiling stage consists of an Induced Gas Flotation (IGF) vessel, which uses micro bubble flotation and Oil Removal Filters (ORF) made from walnut shells that have a high affinity for oil. At this stage, the hydrocarbon content in the water is reduced to 10 ppm. This water stream is fed to an evaporator which produces BFW that meets or exceeds the water quality requirements. Concentrated brine and solids are transferred off site for disposal. More than 90% of the produced water is reused. Brackish water is the primary source for the balance of the boiler feed. Conventional drum boilers are used to generate steam to inject into the reservoir.

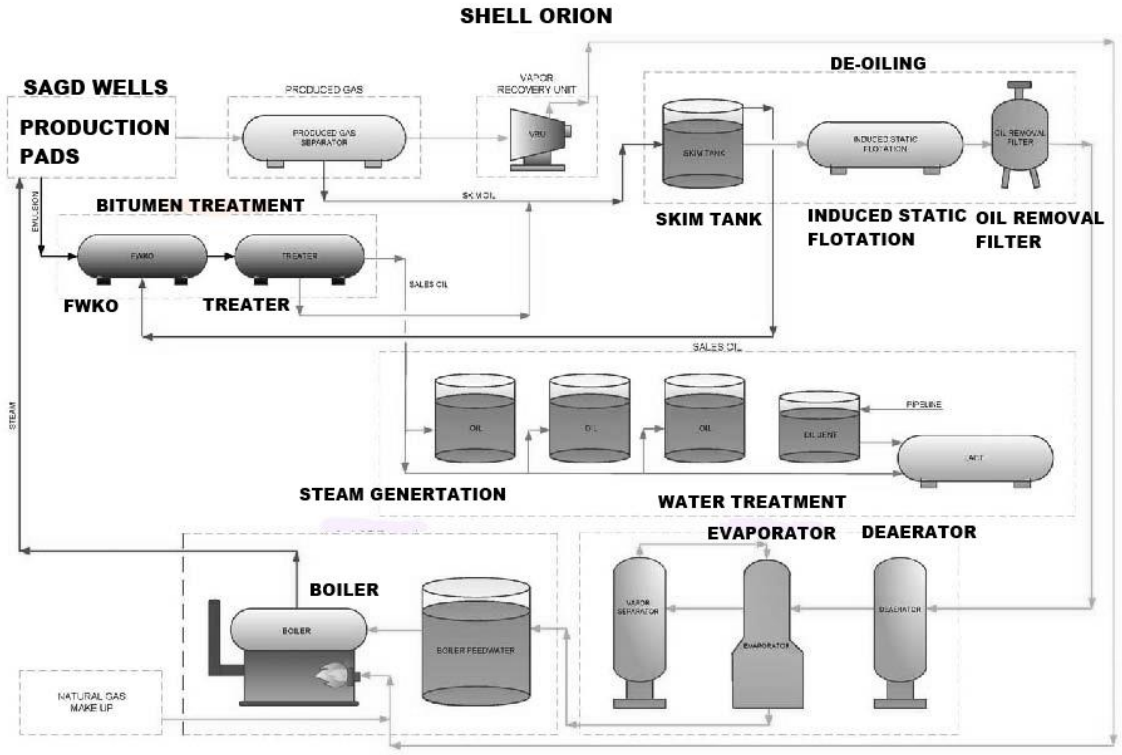

Figure 1-8 Schematic diagram of Shell Orion SAGD produced water treatment process [26]

1.4.2.2 Nexen Long Lake SAGD Facility Case

The schematic diagram of the Nexen Long Lake SAGD surface facility is shown in Figures 1-9 and 1-10. The preliminary and secondary separation processes are identical to the Shell Orion facility. They also use a Free-Water-Knock-Out drum together with an electrostatic grid treater for their preliminary separation. Induced Gas Flotation (IGF) combined with an Oil Removal Filter (ORF) is used for the secondary de-oiling process. The ORF provides final upgrading of the water by reducing the oil content to 5 ppm. The deviation from the previous scheme begins at the water treatment stage where a conventional method is used. Produced water is fed to the Hot Lime Softening (HLS) and Weak Acid Cation (WAC) processes to reduce the magnesium and calcium from the water to the water quality criteria. Finally, produced water is pumped into the Once Through Steam Generator (OTSG) to generate steam for re-injection.

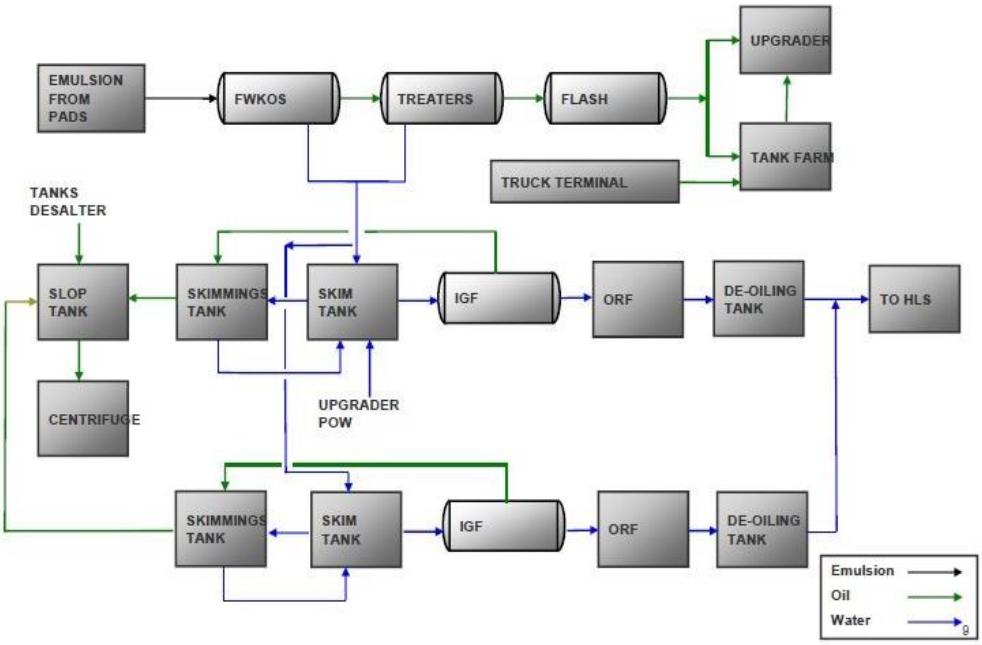

Figure 1-9 Schematic diagram of the Nexen Long Lake SAGD produced water treatment process (before the hot lime softening process) [27]

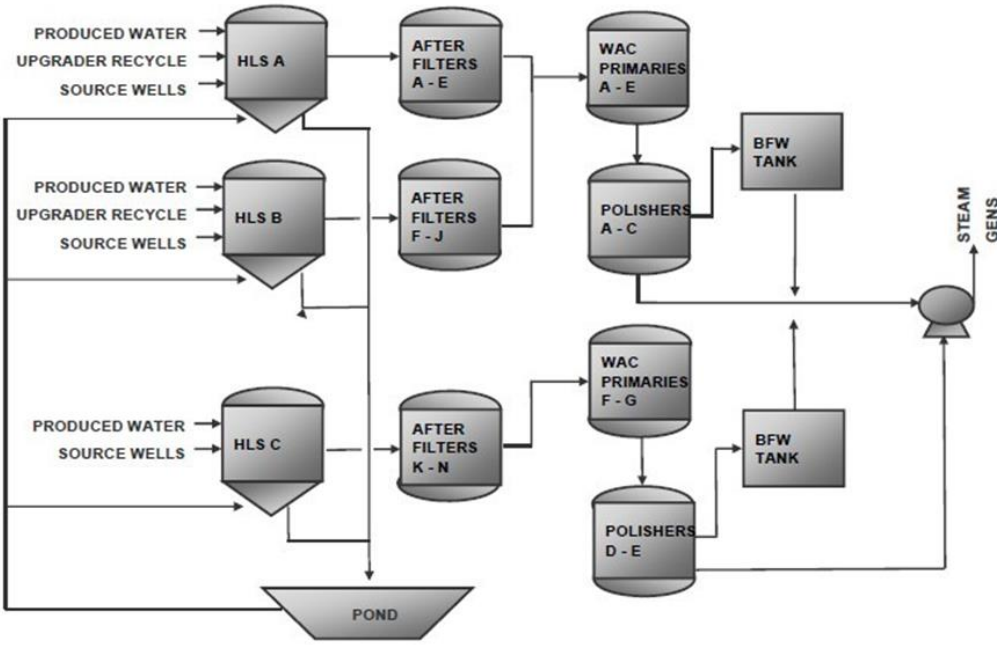

Figure 1-10 Schematic diagram of the Nexen Long Lake SAGD produced water treatment process (after the hot lime softening process) [27]

1.4.2.3 ConocoPhillips Surmont SAGD Facility Case

Figure 1-11 shows a schematic diagram of the ConocoPhillips Surmont SAGD produced water treatment process. The Surmont SAGD facility is similar to the Nexen Long Lake SAGD process. A skim tank combined with an Induced Gas Flotation (IGF) comprises the de-oiling process and Warm Lime Softening (WLS) together with the Weak Acid Cation (WAC) for the water treatment. Finally, the produced water is pumped into the Once Through Steam Generator (OTSG) to generate steam for re-injection.

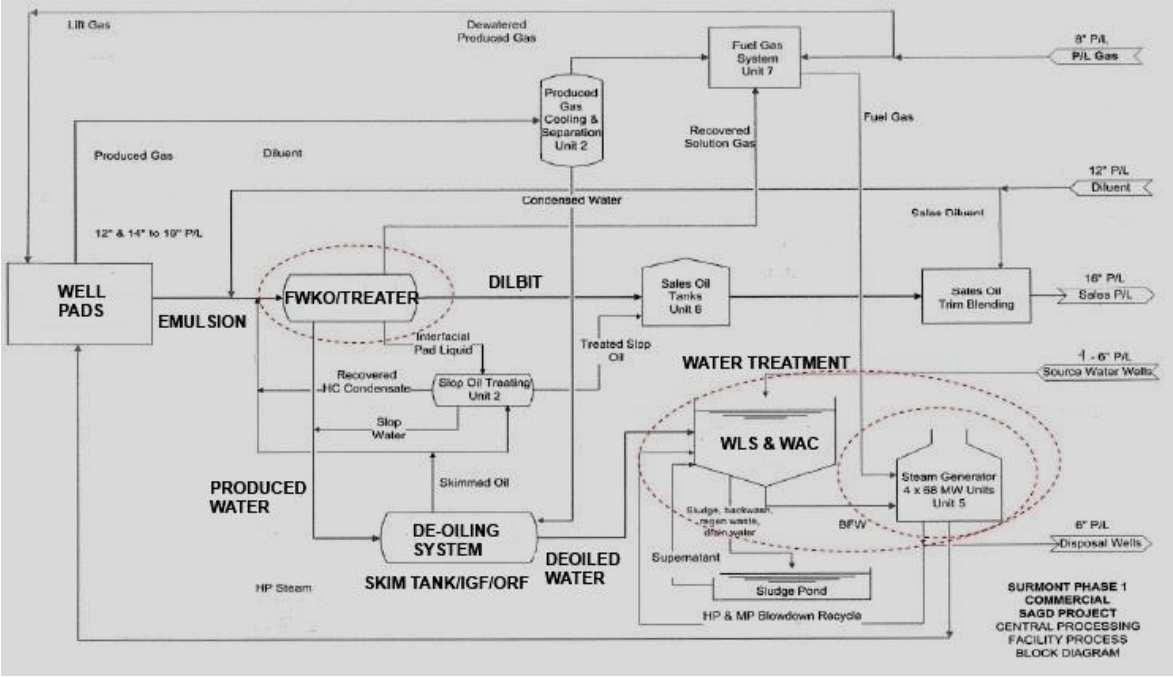

Figure 1-11 Schematic diagram of the ConocoPhillips Surmont SAGD produced water treatment process [28].

1.5 Multiphase Flow Mechanics and Phase Separation in Oil Sand Production

The phase interactions among bitumen-water-gas (in situ produce) and solid (mining produced) bitumen are important to researchers and practitioners involved in SAGD and surface mining process operation and development. Understanding emulsion formation/breakage, dispersion, and mass and heat transfer phenomena linked to these complicated systems provide practical means to optimize process operation or design to maximize bitumen recovery, minimize the water and solid content in bitumen product as well as to minimize energy requirements and to meet environmental regulations.

1.5.1 Batch Gas-agitated Liquid-Liquid Systems

A simplified batch gas –agitated liquid-liquid system was studied by Konduru and Shaw [29].The initial stratified layers are formed by two immiscible liquids with different densities, the bottom more dense phase is an aqueous sugar solution while the upper phase is a mixture of less dense sunflower oil + decane. Bubbles were introduced by injecting nitrogen gas from the bottom of the vessel. As illustrated in Figure 1-12, the liquid from the bottom phase is entrained into the upper phase by the gas bubbles passing through the liquid-liquid interface. Fine drops become suspended in the upper phase. At the end of the batch, the gas flow is stopped and the majority of the fine drops transfer back to the bottom phase. A small fraction of the lower liquid remains in the upper phase and forms dispersion.

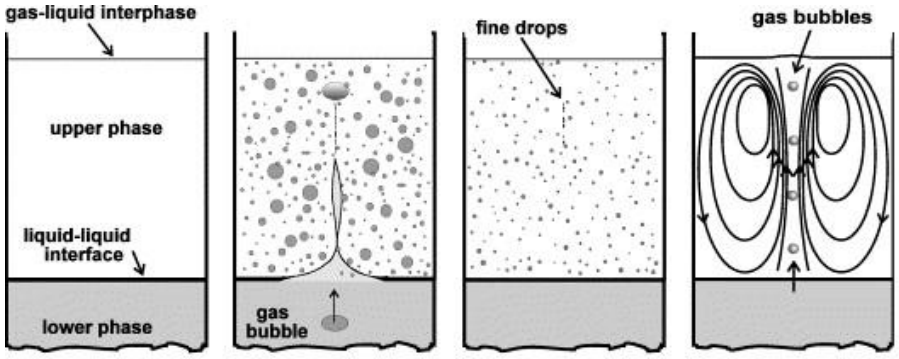

Figure 1-12 The formation and evolution of batch gas-agitated liquid-liquid dispersions [30]

By analogy, the liquid crystal-rich domains, present in bitumen, may transfer to the water-rich phase by a comparable transfer mechanism, as shown in Figure 1-13. This process is governed by the interaction of gas bubbles passing through the liquid-liquid interface from the bitumen-rich phase to the water-rich phase. Liquid crystal domains, known to be surface active, adhere to the bubbles, Figure 1-13 (a), and are entrained with the bubbles across the interface as into the water-rich, Figure 1-13 (b) and (c), even after the bubbles burst at the water-vapour interface Figure 1-13 (d). For this case the orientation of the phases and the interface itself are not static but the principles transport are similar and this or a related mechanism may be active.

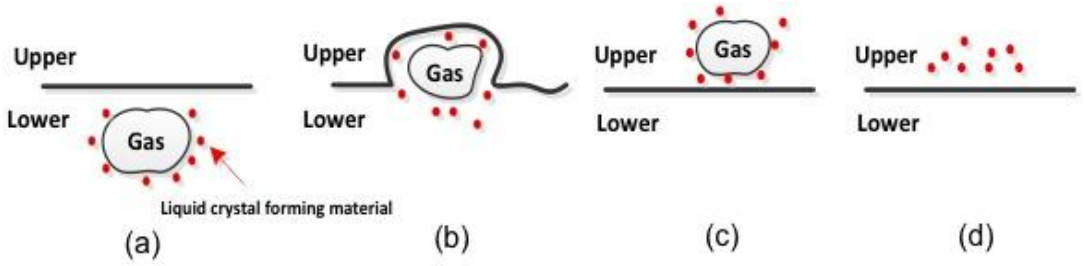

Figure 1-13 Conceptualization of liquid crystal transfer across a liquid-liquid interface in gas-agitated liquid-liquid dispersions.

1.5.2 Flotation Cell System

Flotation combines physical, chemical and physicochemical phenomena and this process is widely used in to remove solid particles from water in the mining industry. In the oil sand industry, flotation is used in primary separation vessels (PSVs) after the oil slurries are hydro transported from the pit to the extraction plant where bitumen and gas bubbles interact. The attachment of bitumen to the bubbles induces a density difference and allows the bitumen to float to the top, so when the aerated bitumen water slurry is fed into the flotation vessels, it is stratified into three layers: bitumen froth, a middling layer and an underflow, as shown in Figure 1-14.The boundary between upper froth and middling zone is usually a multi-emulsion region consisting of water, bitumen and solid, known as a rag layer.

From a micro-scale view, bitumen attaches the air bubbles due to the hydrophobic nature of the hydrocarbons. At high temperature, the air bubbles become completely engulfed by bitumen and the best separation is achieved. Bubble size and bubble size distribution play a critical role in the overall flotation performance and there is a limit on the size of bubbles that can be engulfed by bitumen at various temperatures. The maximum size is called the critical bubble diameter and it increases with temperature up to 45°C. The whole process is represented by stage (F) to (H) in Figure 1-15.

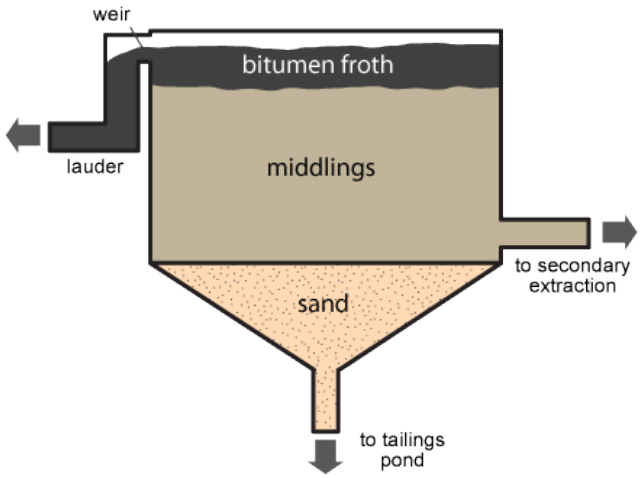

Figure 1-14 Primary separation of bitumen occurs in the primary separation vessel

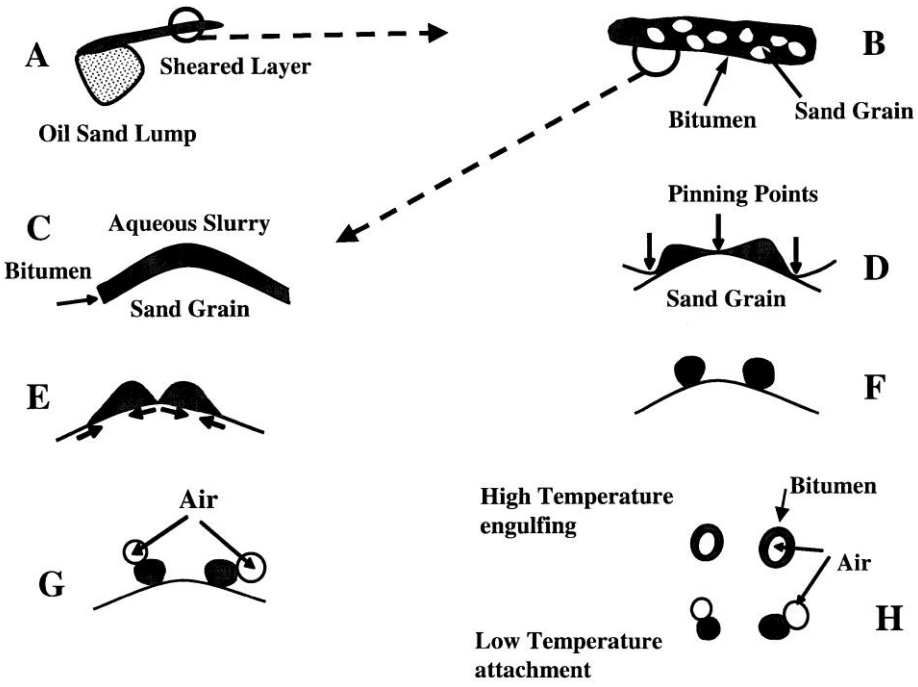

Figure 1-15 Illustration of the bitumen liberation and aeration [11]

During primary separation of mined oil sands ore, liquid crystals have been discovered largely in the rag layer. The presence of these domains at the water/oil interface has been thoroughly discussed in section 1.3.3. However, at the initial stage, the potential role of these entrained domains on the bubble coalescence and froth stability is yet unknown. As shown in Figure 1-16 (a), these surface active hydrocarbon domains, which are

hydrophobic, are easily captured by the gas bubble in the middling zone and brought up to the rag layers. As bubbles rise, these materials tend to accumulate in the rag zone in the flotation cell, shown in Figure 1-16 (b). And the mechanism of the collision and aggregation of bubbles in this region may change be affected by the presence of these domains. They may act as a bridging material between bubbles that leads to the formation of bubble clusters as two bubbles may become connected by these hydrophobic domains or bubbles may be covered by the hydrophobic domains first and then cluster together due to the aggregation of these domains. Also they may interact with the bitumen froth from the upper phase and some of them may be recaptured by the bitumen froth phase as the bubbles burst. However, further investigation is needed, as these potential mechanisms are unproven.

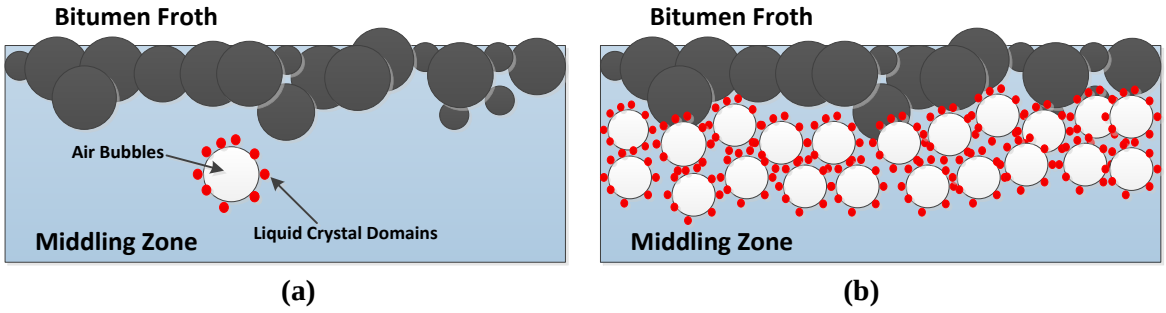

Figure 1-16 Conceptualization of liquid crystal transfer in flotation cell

1.6 Objectives and Thesis Outline

This work is intended to improve the understanding of the composition and the fate of organic liquid crystal derived from raw bitumen during production. As liquid crystals appear to have been observed in the rag layer of separation vessels associated with mined bitumen, the focus of this work is on their fate during SAGD production. Both laboratory scale batch experiments and field scale SAGD measurements are envisaged. Development of scalable methods for isolating liquid crystals is a second objective.

Based on the targeted objectives, this thesis is structured as follows. Chapter 2 concerns a laboratory study intended to simulate the fluid mechanics and temperature regimes associated with SAGD production. Possible liquid crystal transfer mechanisms are discussed. Chapter 3 comprises a field study related to the fate of liquid crystals in SAGD

surface facilities. Chapter 4 concerns the development of a scalable method for isolating liquid crystals. It is based on their separation from the water phase and exploits their surface activity. Chapter 5 comprises the conclusions and recommendations for possible further work.

Chapter 2 Observation of Liquid Crystal in Heated Water + Athabasca Bitumen

2.1 Introduction

Bitumen, which is a complex ill-defined mixture, consists of thousands of compounds including light to heavy hydrocarbons and some heteroatomic molecules (S, N, O, metals, etc.) [31]. It is fractionalized into boiling ranges, or into four solubility-based groups: saturate, aromatic, resin and asphaltene, known as SARA fractions [32] used here. The maltene fraction includes the saturates, aromatics and resins fractions. As mentioned in Chapter 1, liquid crystal–rich domains were recently discovered in both the C_5 asphaltene and C_5 maltene fractions [8]. Mechanistically this can be interpreted as one axis of a fraction of the molecules present in these two fractions tend to align along a preferred direction [33]. The focus of this chapter is to determine these domains transfer from the bitumen-rich phase to the water-rich phase.

2.2 Materials

Athabasca Bitumen (abbreviated as AB) was supplied by Syncrude Canada Ltd. It was obtained after a series of mining processes (warm-water extraction, naphtha dilution and naphtha recovery by distillation). The sample was characterized as a coker feed and volatile compounds are lost to some extent during sample preparation. The detailed properties (including elemental composition and SARA analysis) of Athabasca bitumen used in this work are listed in Table 2-1 [34].

Table 2-1 Detailed properties of Athabasca bitumen

Composition	Athabasca Bitumen
	Mass Fraction (%)
C	0.832
H	0.097
S	0.053
O	0.017
N	0.004
Saturates	0.161
Aromatics	0.485
Resins	0.168
C_5 Asphaltene	0.186
	Metal Analysis/mg · kg^{-1}
Al	492
Ba	6.4
K	77
Ca	163
Cr	2.8
Fe	762
Mg	65
Mn	30
Mo	12
Na	91
Ni	93
Si	355
Ti	24
V	247
Zn	4.4

HPLC grade deionized water (99.99 wt. % purity) was purchased from Sigma-Aldrich. Toluene (99.99 wt. % purity) used for washing a micro reactor was provided by Fischer Scientific. Nitrogen (99.998% purity, supplied by Praxair) and Snoop® liquid leak detectors (provided by Swagelok) were used for leak detection before each experiment.

2.3 Experimental Apparatus

2.3.1 Micro Batch Reactor

The micro reactor used in this study is identical to those used previously for a laboratory scale hydro-processing study [35]. These batch reactors have an upper operating rang of 600 ℃ and 15 MPa; limits well in excess of the conditions explored here. They have an internal volume of ~ 15mL and are constructed from Swagelok parts. The detailed configuration is showed in Figure 2-1. The main body is a 3/4" stainless tube with a thickness of 1/15" and a 3/4"end cap at the bottom. The 3/4"×1/8" reducing tubes are attached on the other side and they are connected by a 1/8" stainless stem tuber with a screwed bonnet needle valve. A thick aluminum bracket is also attached for holding the reactor in position.

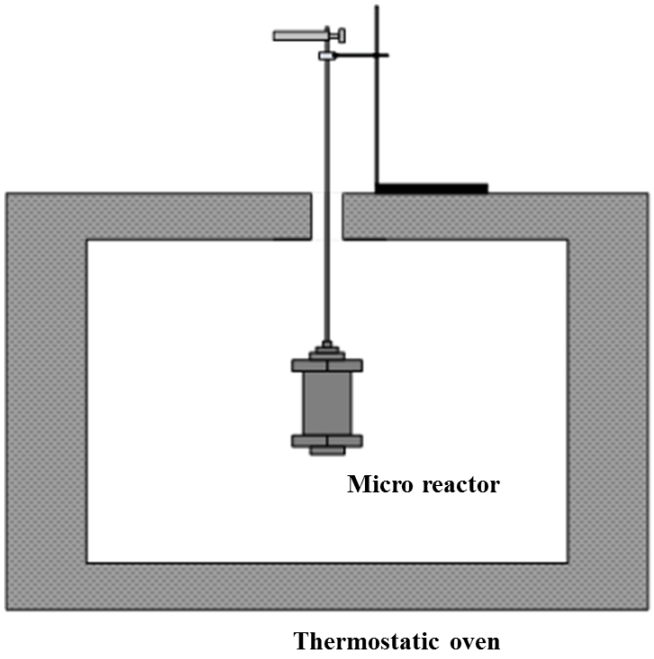

Figure 2-1 Schematic of the micro reactor mixer

2.3.2 The Heating Systems

Two systems were used for heating and then stabilizing the temperature of the micro batch reactor: 1) A furnace system equipped with iron supports which hold the reactor in place; 2) A fluidized sand bath (Tecam Fluidized Sand Bath Model No.SBS–4) with an external agitator to which the reactor may be clamped. These two heating systems provide a choice of static and vertical mixing environments respectively during heating.

2.3.3 Olympus GX 71 Inverted Microscope

An Olympus GX 71 inverted microscope (Figure 2-2) equipped with five different magnification objectives (LM Plan FLN 5x, 10x, 20x, 50x and 100x) and a polarizer (Olympus GX-AN 360) was used to observe samples. An image acquisition system is connected in front of the microscope; image information can be recorded during in situ observation and further processed by the Olympus Stream Software. In this work, both normal light and cross-polarized light modes were applied.

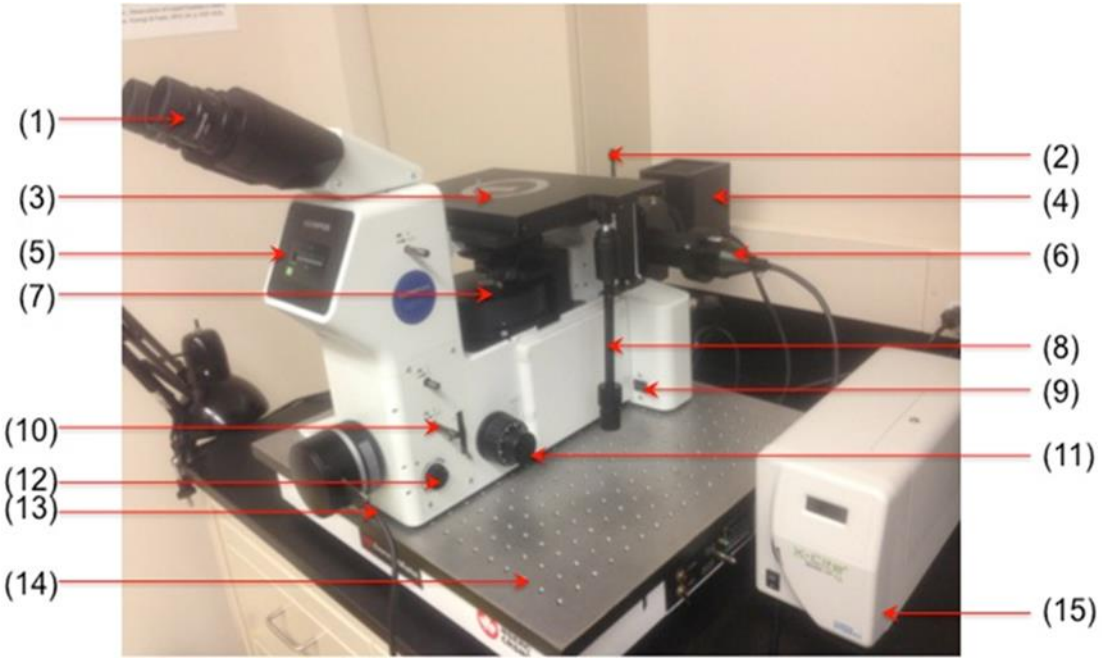

Figure 2-2 The side view of Olympus GX71 microscope: (1) Ocular lens, (2) Illuminator switcher, (3) Mechanical stage, (4) Halogen light source, (5) Light intensity indicator, (6) Fluorescent light connector, (7) Objective lens nosepiece, (8) Stage drive, (9) On/off button, (10) Digital camera switcher, (11) Focus adjustment knob, (12) Light intensity control, (13) Digital camera cable, (14) Anti-vibration stage, (15) Fluorescent light source.

2.4 General Theory of Polarized Light Microscopy

Polarized Light Microscopy (PLM) is used to measure the birefringence of samples [36]. The theory of PLM has been thoroughly discussed in [37]. The basic configuration of PLM is typically an optical microscope with additional two filters in the optical path. The one located after the illumination sources, which is known as a polarizer, is used to ensure that only polarized light is transmitted to the specimen, while the other filter, which is located behind the specimen but in front of the objective lens in the imaging path. The polarizer

and analyzer are in crossed positions so that the polarized light passing through the polarizer will be blocked by the analyzer in the case of an isotropic material and the resulted image is dark. However, anisotropic materials change the direction of polarized light and, a birefringence effect, in this case a distinct “Maltese cross” pattern, is observed, as shown in Figure 2-3.

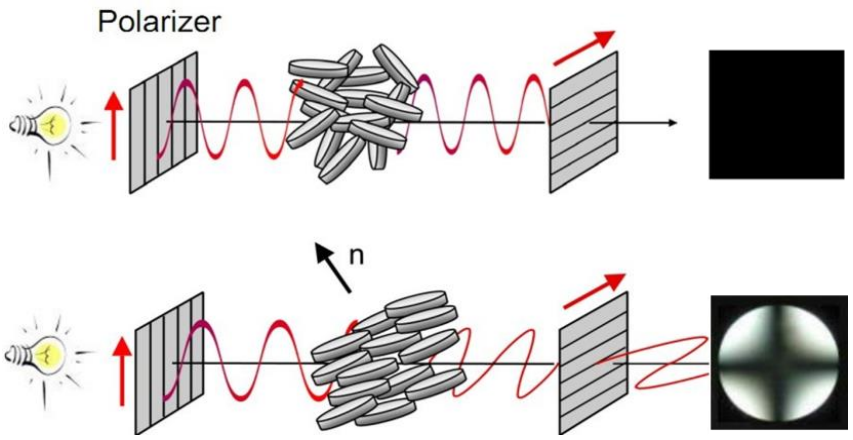

Figure 2-3 A schematic of the principles of cross polarized light microscopy (top: isotropic material under cross-polarized light; bottom: anisotropic materials under cross-polarized light)

This effect is caused by the concentric arrangement of the liquid crystal within the shell, the portions of the shell in line with the axes of the filters are not birefringent, so a well-defined Maltese type cross appears. In many cases, this unique structure under PLM is the most effective way for detecting liquid crystalline materials at the micro scale [33].

2.5 Batch Reactor Operating Temperature Selection

According to the solubility of water in bitumen-rich phase at high temperature [38], the water content in the bitumen-rich phase increases with temperature and can exceed 15 wt.% at 645 K. In order to maximize the solubility of water while maintaining the stability of the reactor during mixing, 593 K was selected as the highest operation temperature, which is also consistent with the steam temperature (573 K~613 K) in the Cyclic Steam Simulation (CSS) process [39]. At this temperature, the solubility of water in bitumen is around 8 wt. %. The pressure is dictated by the vapour pressure of water based on the charge: 2 grams bitumen and 2 grams of water. The water saturation pressure at 593K is 11.27 MPa [40]. At the other two temperatures, 473 K and 523 K, which are in the range of the conventional temperature of steam generated and re-injected in the typical SAGD

processes, the pressures inside of the micro reactor are 1.55 MPa and 3.97 MPa, respectively [40].

2.6 Batch Reactor Mixing Procedures

The Athabasca bitumen was first placed in a Fischer Scientific Isotemp Oven for preheating at 70°C for ~30 minutes before it was loaded in the micro reactor. This temperature was selected for two reasons: to decrease viscosity of bitumen for easier loading, and at the same time the density of bitumen is reduced to ~0.969 g/ml at that temperature [41], which is less than the density of water.

Around 2 grams of deionized water was first loaded at the bottom of the micro reactor by syringe at room temperature and then around 2 grams of 70°C preheated bitumen was carefully placed with a spatula on the top of water. The oil–to-water mass ratio was approximately 1.0.

After loading, the reactor was sealed and then pressurized with nitrogen to 11 MPa (maximum experimental pressure condition) for to test for leaks. The reactor was left attached to the nitrogen cylinder for a while to ensure no pressure drop happened. Meanwhile, the Snoop liquid was sprayed around each connector to check for possible leaks. This step was repeated several times until the seal was confirmed. A follow-up depressurization was conducted by the vacuum pump for about 10 seconds to remove nitrogen and residual oxygen in order to minimize oxidation. The amount of water that evaporates during depressurizing stage is negligible.

The reactor was inserted into a furnace (shown in Figure 2-1) or clamped to an external agitator and immersed in a fluidized sand bath kept at the required operating temperatures. According to Peng's study on the temperature profile in the micro reactor [42], the reactor reached the steady state at temperature 696 K within 5 minutes of insertion into the heating system. With the same size and configuration, it was assumed that the reactor reached a steady state temperature (593 K, 523 K or 473 K) in 5 minutes or less, so the time was counted down 5 minutes after the micro reactor was first inserted into a heating system. After the preset time (30 minutes) elapsed, the reactor was removed from the furnace and allowed to cool down to the room temperature in the fume hood. The water phase stayed

on the top of the bitumen and was collected in vials using a syringe. The recovery rate of water was calculated as the equation below:

$$\text{Water Recovery Rate} = \frac{m_{collected\ water}}{m_{initial\ loaded\ water}} \times 100\%$$

The water rich samples were placed in a dark drawer for storage and further analysis.

2.7 Microscopic Analysis Procedures

The water-rich phase liquid samples were placed on glass microscope slides (3"×1"×1mm) before placing on the observation stage. The observations were conducted in the open air environment with room temperature ~25°C and humidity ~33%.

After the microscope illumination system was stable the lowest magnification (5×) was used to focus light on the sample. Then, higher magnifications (10×, 20× or 50×) were applied for detailed observation.

The light intensity was adjusted for different light conditions: for normal light mode, ~5V light intensity was applied for observations; for polarized light mode, higher light intensity (~12V) was needed for light loss compensation upon polarization.

If cross-polarized light observation was needed, a polarized light filter was inserted and rotated slightly until the background was totally black. If anisotropic ordered materials existed in the sample, visible brightness was observed at that time.

After visually checking through the eyepiece, live were transferred from the camera to the computer for storage and possible further analysis. The contrast of the images was digitally enhanced through Image J software. Other image processing was conducted through a variety of software, such as Photoshop, Olympus Stream, etc.

2.8 Repeatability Analysis and Possible Error

Duplicate tests were conducted at each condition. In order to avoid the possibility that the oil drops in water form clusters which could appear as anisotropic regions due to the light reflected from the drop interface and inevitably give bright spots regardless of sample orientation, all the duplicates samples were placed on a vortex mixer for re-mixing prior to observation and the sample slides were rotated 3~4 times manually on the observation stage [18].

The Olympus GX 71 system is equipped with a halogen light source possessing a wavelength in the range of 650 nm to 950 nm. This wave length is one order of magnitude smaller than the objects (~ 5 μm) of interest. However, at high magnification, a scattering halo arises that leads to an over estimation of domain size especially for smaller objects when polarized light is employed. The effect is amplified when several smaller objects are close to one another, due to a multiple scattering effect. In this work, the impact of the halo effect is small and it was only detected at high magnification (the scale bar is 2 μm) as illustrated in Figure 2-4. Under polarized light, Figure 2-4(a), the liquid crystal domain has a diameter of 3.9 μm but the halo around creates the illusion of a larger apparent diameter of 4.2 μm. This is more obvious optically when Sobel boundary detection is applied, as shown in Figure 2-4(b). Errors introduced by the scattering halo, aperture size and magnification, may be ignored in the context of the present work because the actual diameter of objects is a few percent, at most, smaller than the apparent diameters under the most unfavourable conditions.

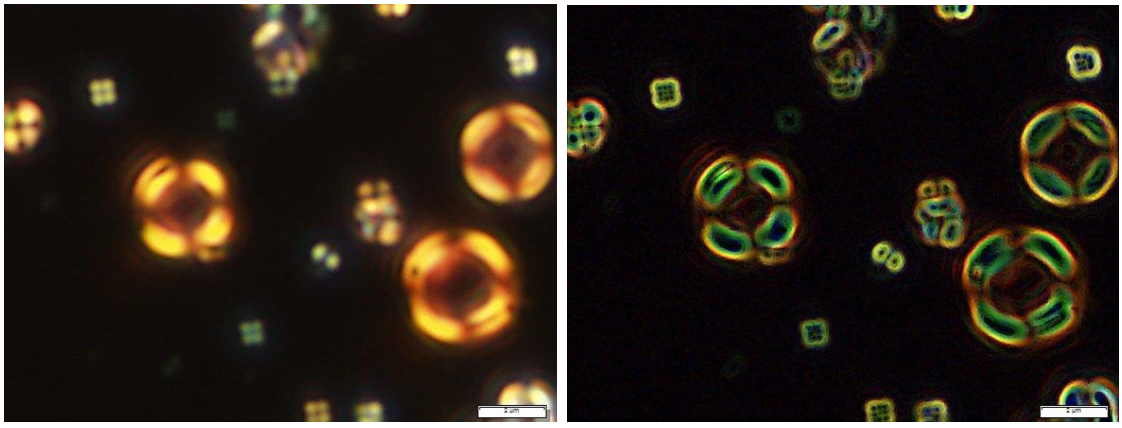

(a) **(b)**

Figure 2-4 The scattering halo of a liquid crystal domain under high magnification. (a) under polarized light; (b) using Sobel boundary detection. (The scale bar is 2 μm.)

2.9 Results and Discussions

2.9.1 Liquid Crystal Domain Static Structure and Formation Study

Under cross-polarized light, liquid crystals with isotropic cores, covered by an anisotropic shell [43], exhibit the typical "Maltese Cross" pattern. Figure 2-4 shows that the "Maltese Cross" domains are dispersed in the water phase obtained from water + bitumen samples

heat treated at 593 K and cooled to room temperature. They are consistent with other organic molecules forming a liquid crystalline texture described in the literature [44, 45]. Comparing the structure of liquid crystals in the water phase with those from different original hydrocarbon sources (shown in Figure 2-5), it can be concluded that their structures are identical.

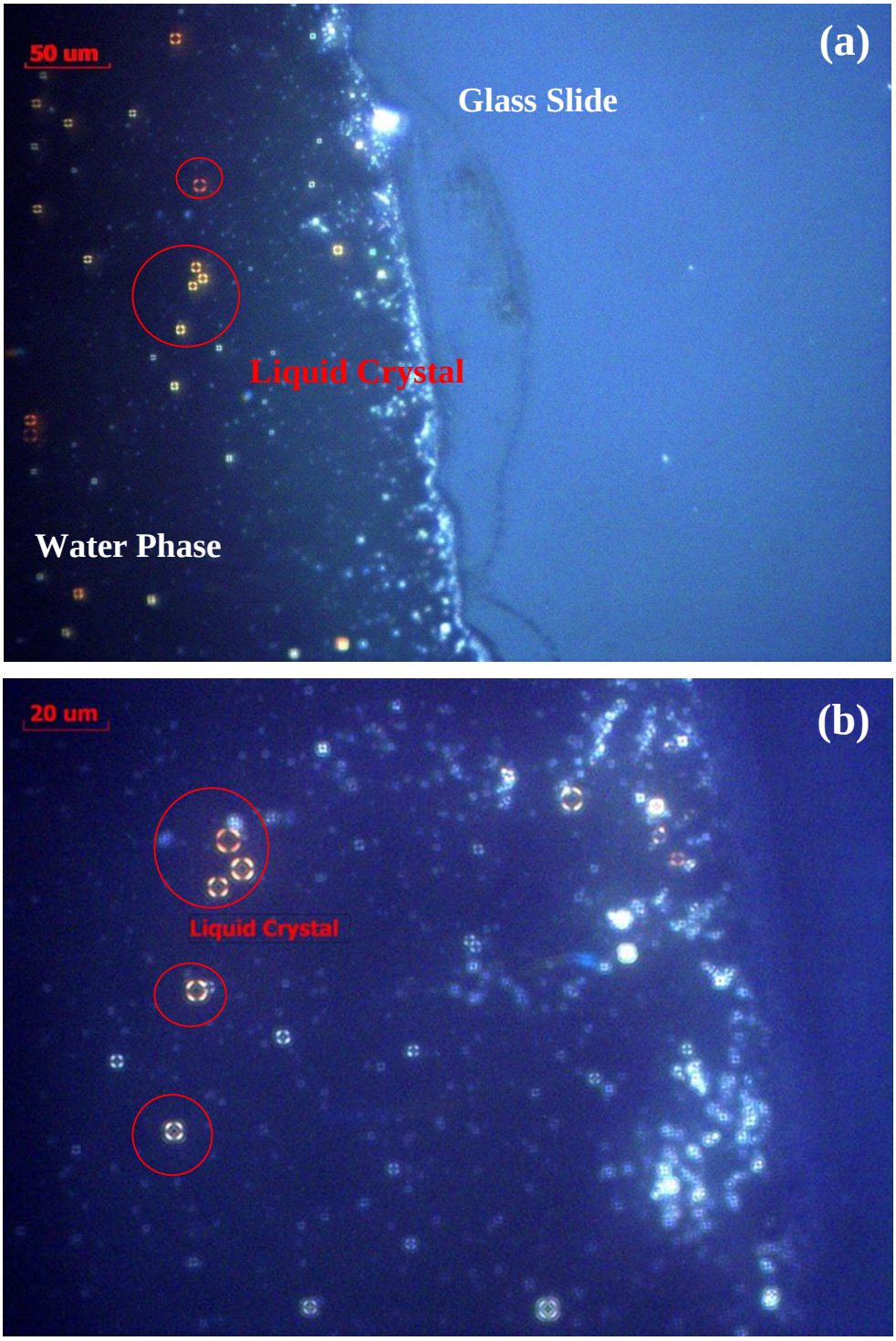

Figure 2-5 Images of a water-rich sample under cross-polarized light immediately after it was collected: (a) 20x magnification, (b) 50x magnification. Typical liquid crystal domains are highlighted with red circles. Note: the contrast of the images was enhanced through Image J.

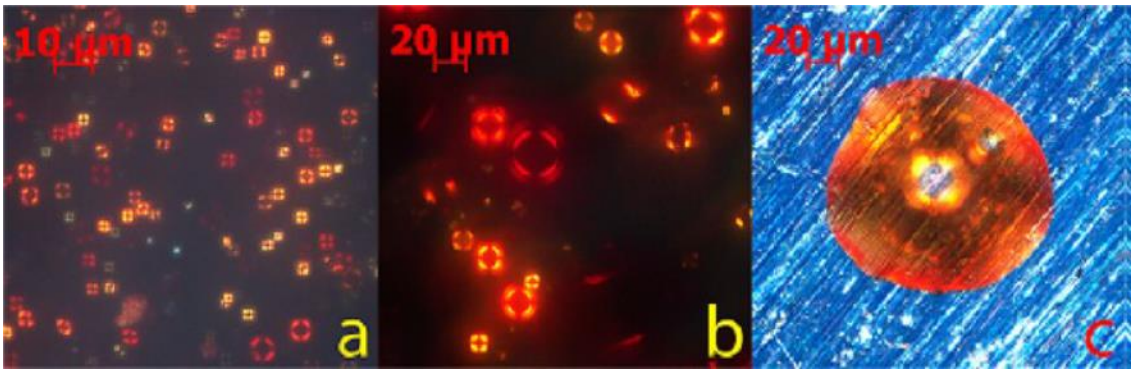

Figure 2-6 Images of liquid crystal domains from different sources under cross-polarized light: (a) Athabasca C_5 asphaltenes, (b) Fraction of vacuum residue extracted using supercritical pentane, known as the SFE6, and (c) Athabasca C_5 maltenes [7]

It is worth noting that the formation process for liquid crystal domains in these different cases may differ. For C_5 asphaltenes, the sample was crushed and placed on glass slides for observation. The liquid crystal layers formed on the surface of the particles upon heating, which, at the molecular scale, means that liquid-crystal forming molecules diffused and then ordered on the surface when temperature increases. In C_5 maltenes, the liquid crystals were suspended in the isotropic liquid when they appeared. Although they formed a separated phase different from the core and surrounding, it is hard to conclude whether the liquid-crystal forming molecules anchored and ordered from the exterior or interior surface. However for the water-separated samples, three phases are involved, which makes it more complicated. Both mechanical and thermal driving forces contribute to the formation of liquid crystals. This aspect is discussed in section 2.9.4.

Diameter is another characteristic for describing the morphological structure of liquid crystals. According to Masik's study, the diameters of domains combined with the number of domains could be related to the quantity of the liquid crystals [9]. In the variety of oil phases studied, the diameters of the domains are governed by viscosity of the forming material, so the domains in Athabasca C_5 asphaltenes are relatively smaller than those in Athabasca C_5 maltene [7]. The diameters of liquid crystal domains in the water rich phase are from 2.4 µm to 5.6 µm, which is one order of magnitude smaller than those found in the original resource fractions (Table 2-2).

Table 2-2 Diameter of liquid crystals found in different resource fractions

Liquid Crystal Sources	Diameter (μm)
Athabasca C_5 maltene	~50
SFE6	~40
Athabasca C_5 Asphaltene	~10
Water-rich extract	2.4~5.6

2.9.2 Liquid Crystal Domain Mobility in the Water Phase

The liquid crystal domains in C_5 asphaltenes, which are formed at the edges of particles attached to the glass or aluminum slide, are similar to the liquid crystals in C_5 maltenes, which are surrounded by relatively viscous isotropic fluid. They are both at rest position during observation. However, the liquid crystal domains in the water-rich phase are mobile both in the bulk and on the rim and tend to concentrate on the rim of sessile water drops, as shown in Figure 2-6 (d). This effect is accentuated as the sessile drops evaporate. After the water evaporates, the liquid crystal domains remain dispersed on the slides as shown in Figure 2-6(c).

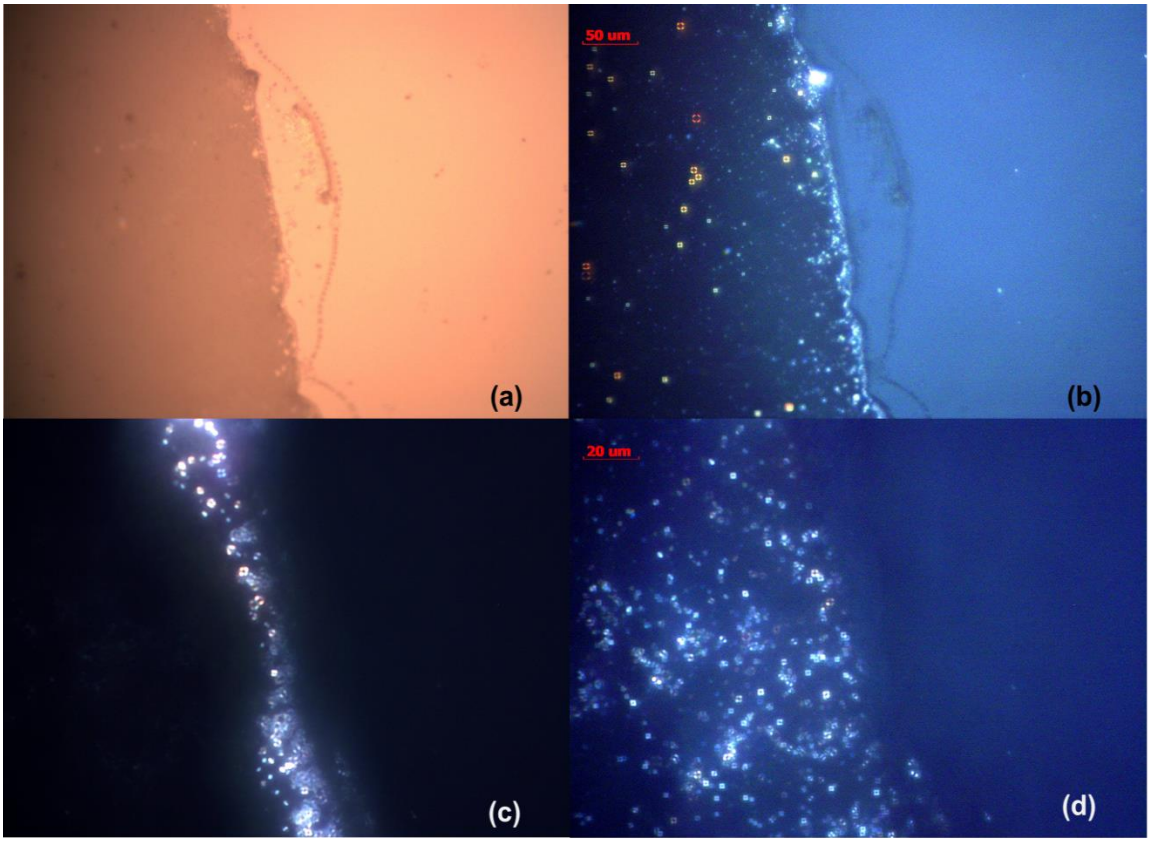

Figure 2-7 Images of a water-rich sample under reflective normal light (a) and cross polarized light (b, c and d) at room temperature and atmospheric pressure: (a) Rim area under normal light; (b) Rim area of the liquid crystal containing water sample under cross-polarized light; (c) The sample after the water has evaporated; (d) The sample before water was evaporated. Images (a) and (b) are at the same magnification. The scale bar is shown in (b). Images (c) and (d) are at the same magnification. The scale bar is shown in (d).

2.9.3 Liquid Crystal Stability in the Water Phase

The role of liquid crystal domains at the oil-water interface has been reported by Czarnecki and coworkers [19, 46, 47]. According to these studies, liquid crystals enhance the stability of an emulsion or foam by coating oil drops with liquid crystal layers in water, which increases the rigidity of the interface and prevents fingering [48] and inhibits dewatering in the froth treatment process. In this work, the liquid crystal domains remain stable for at least three months, as shown in Figure 2-7, where following three months of aging, the liquid crystal domain size remains unchanged.

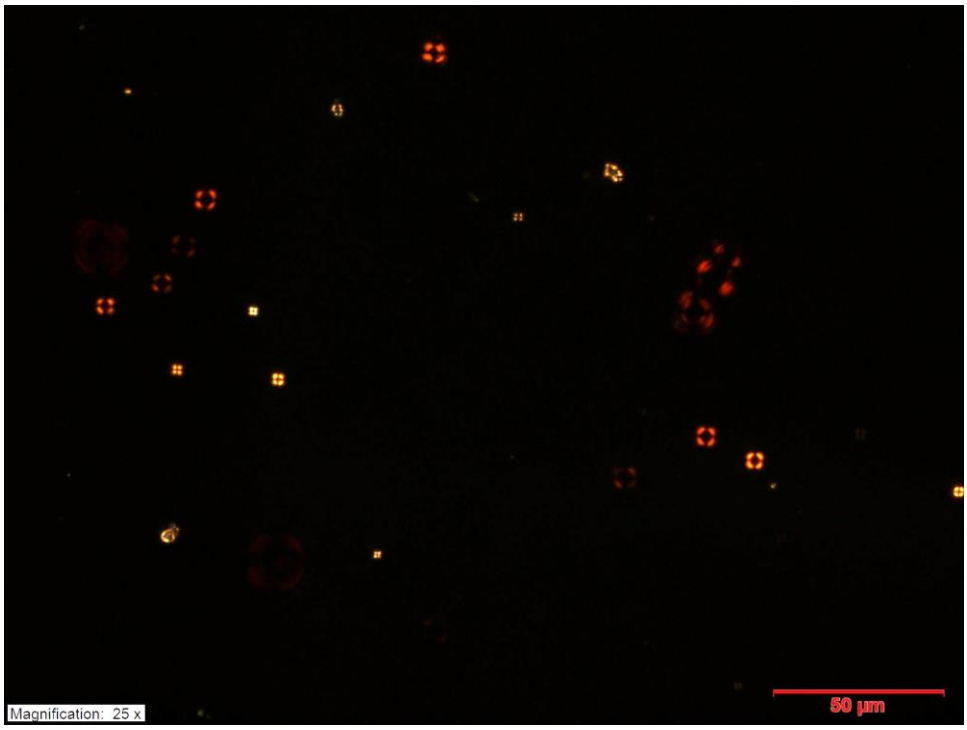

(a)

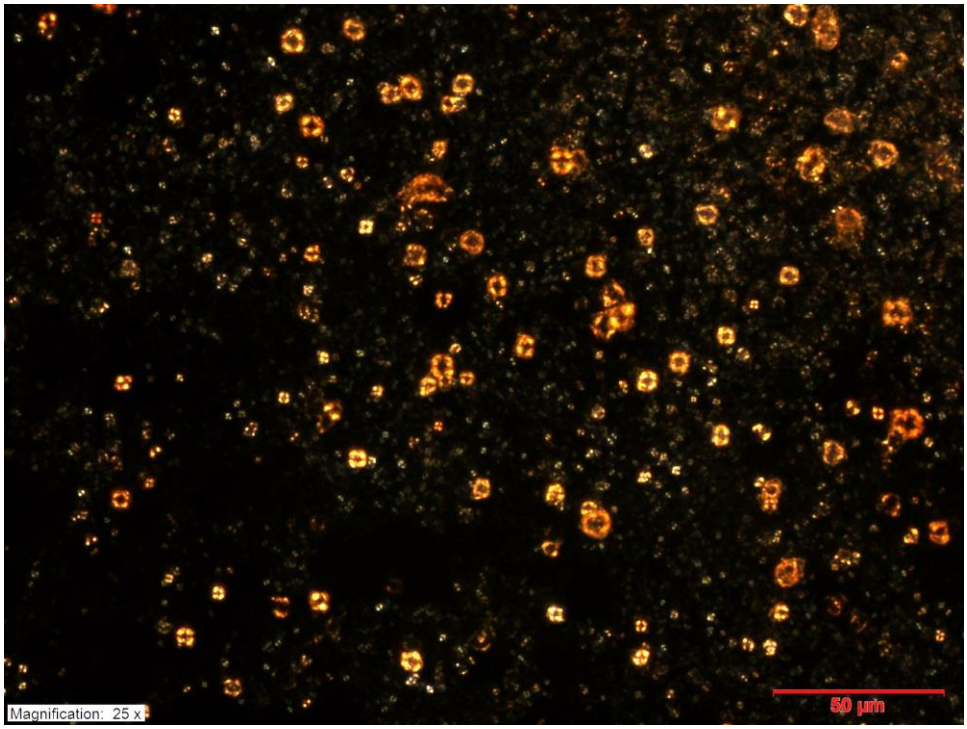

(b)

Figure 2-8 Liquid crystals in a water sample under cross polarized light from the same batch as in Figure 2-4 after three months, indicating the stability of the liquid crystal domains: (a) Before the water was evaporated; (b) After water evaporation.

2.9.4 Possible Liquid Crystal Domain Transfer Mechanisms

The transfer mechanism for liquid crystal domains from the bitumen rich phase to the water rich phase is not known a priori and in situ observation remains infeasible. Possible mechanisms are identified here. As clearly described in Section 2.6, the bitumen was preheated at 70°C for 30 minutes. Although the density of bitumen was lower than that of water, the difference was not significant. So when water was loaded into the reactor first followed by bitumen, the bitumen was partially or full immersed into the water phase and a water-bitumen interface was generated in the micro reactor. Some water would be present at all elevations initially. For three experiments the micro reactor was suspended in an oven (no external agitation). For three additional experiments, the micro reactor was shaken vertically with an amplitude of 3cm at 3Hz. As shown in Table 2-3, liquid crystal domains were present in the water-rich phases for all six experiments. Despite the difficulty in quantitating the extraction efficiency of the liquid crystal domains, the structure and size of the domains 2.4 μm~ 5.6 μm is unaffected by this variation and operating temperature variation. As the transferred liquid crystal-rich domains are also an order of magnitude smaller than the average domains arising in Athabasca Bitumen, these observations allow for the following possible transferring mechanisms:

1. There is sufficient agitation induced by water evaporation to yield the same outcome in all six cases via a hydrodynamic mechanism during initial heating to 473 K, as outlined in the introduction.
2. There is sufficient volatilization of bitumen constituents below 473 K to entrain liquid crystal domains into the water rich liquid directly as the bubbles pass through the water rich phase or indirectly as bitumen bubbles burst at the bitumen vapour interface and the domains drop into or on the liquid water phase as illustrated in Figure 2.8
3. The transfer occurs on cooling, below 473 K, as dissolved water transfers from the bitumen-rich phase to the water-rich phase.
4. Mobile liquid crystal-rich domains move to the bitumen-water interface and transfer by some other mechanism, possibly, driven by other interfacial, or thermodynamic phenomena independent of water or light hydrocarbon transfer.

Table 2-3 Summary of liquid crystal extraction tests

Test No.	Temperature/K	Pressure/MPa [40]	Time/ Minutes	Vertical mixing	Liquid Crystals in Water Phase
1	473	1.55	30	3Hz	Present
2	523	3.97	30	3Hz	Present
3	593	11.27	30	3Hz	Present
4	473	1.55	30	–	Present
5	523	3.97	30	–	Present
6	593	11.27	30	–	Present

None of these mechanisms can be precluded on the basis of the data in the literature for model systems [29, 49], or for mixtures containing bitumen [50], and they are all plausible.

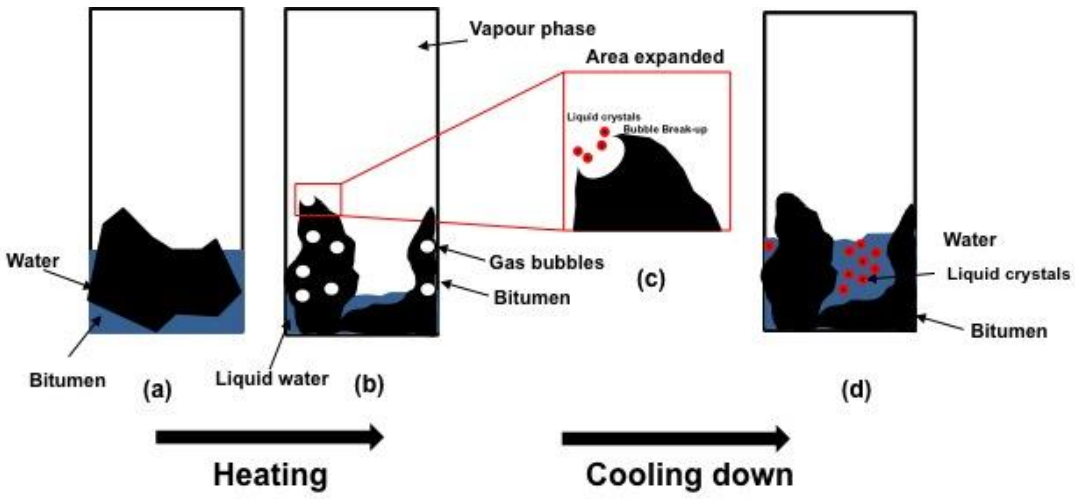

Figure 2-9 Sketch of a hypothetical liquid crystal domain transfer mechanism in a static reactor exposed to high temperature: (a) bitumen water and gas phase are in direct contact with each other at the initial stage of the heating; (b) liquid crystal domains are entrained into the water rich liquid and the vapour as the bubbles pass through the bitumen-vapour and bitumen-water interfaces; (c) bitumen bubbles burst at the bitumen vapour interface and the domains drop into or on the liquid water phase; (d) dissolved water transfers from the bitumen-rich phase to the water-rich phase.

2.10 Summary

These measurements show that liquid crystal domains arising in the bitumen-rich phase are transferred to the water-rich phase of water + Athabasca bitumen mixtures heated to the in-

situ operation temperature conditions (473 K, 523 K and 593 K) and then cooled to room temperature, whether or not the samples were subjected to forced agitation.

The structure of the liquid crystals was identical to those identified in the original hydrocarbon-rich phases. The diameter of the liquid crystals in the water phase ranged from 2.4 μm to 5.6 μm, one order of magnitude smaller than the average size observed previously in the hydrocarbon-rich phase.

The liquid crystal domains are mobile in the water-rich phase and tend to concentrate at the rim of sessile droplets of water. This effect is accentuated as water evaporates.

The mechanism for transferring liquid crystal domains from the bitumen-rich phase to the water-rich phase remains unresolved. None of a number of plausible mechanisms can be precluded on the basis of available data.

Chapter 3 Fate of bitumen derived organic liquid crystals in SAGD surface facilities

3.1 Introduction

Organic liquid crystal domains, comprising an anisotropic shell surrounding an isotropic core, were observed in unreacted heavy fractions extracted from Athabasca bitumen and other bitumen derived hydrocarbon resources [7, 8]. Transfer of these dispersed and surface-active hydrocarbon domains from Athabasca bitumen to a water-rich phase was demonstrated during laboratory trials as described in detail in Chapter 2.

As more than 80% of the northern Alberta oil sands and heavy oil are too deep to mine and must be recovered by *in situ* methods [20] , it is important to understand the fate of these liquid crystals in the water-rich phase in the surface facilities associated with SAGD and other water intensive production processes. Their presence may cause unanticipated technical challenges arising from their deposition or rupture that: (1) may complicate water re-use and disposal, (2) may affect the choice of chemical or other treatments used to reduce hydrocarbon content in recycled water streams. The possible value, toxicity and other thermophysical properties of the liquid crystalline materials are also unknown. In this preliminary field study, six samples from industrial SAGD facilities (Shell, Nexen, ConocoPhillips), were analyzed to determine whether organic liquid crystals are present in the water-rich phase found in industrial SAGD processes, and if so whether and where they are eliminated from the water-rich streams in the surface facilities.

3.2 Materials and Methodology

3.2.1 Materials

Six samples, A-F, were obtained from SAGD facilities in Alberta. The sample sources are summarized in Table 3-1 and the sample appearances are shown in Figure 3-1. The approximate sample points within the surface facilities are illustrated in Figure 3-2.

Samples D and E from Shell were stored for 10 years, while samples A-C and F were obtained recently and were forwarded for analysis following sampling.

Figure 3-1 Bulk appearance of samples A to F (from left to right)

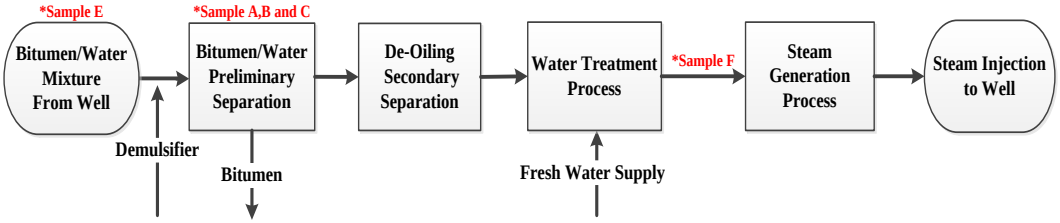

Figure 3-2 Simplified schematic of SAGD water treatment processes showing the sample points for samples: A, B and C, Parallel Feed Water Knock Out (FWKO) drum produced water; E, produced water/bitumen emulsion; F, polished water before entering the Once Through Steam Generator (OTSG).

Table 3-1 Water sample sources

Sample ID	Sponsored Company	Plant Location	Sampling Point	Phase State	Color	Smell
A	Nexen Inc.	Long Lake	Free Water Knock-Out Drum A	Liquid	Straw color to clear	Slight hydrocarbon odor
B	Nexen Inc.	Long Lake	Free Water Knock-Out Drum B	Liquid	Straw color to clear	Slight hydrocarbon odor
C	Nexen Inc.	Long Lake	Free Water Knock-Out Drum C	Liquid	Straw color to clear	Slight hydrocarbon odor
D	Shell	Orion	Not Available	Liquid	Colorless	Slight hydrocarbon odor
E	Shell	Peace River	Not Available	Emulsion	Black color	Strong hydrocarbon odor
F	ConocoPhillips	Surmont	Low Pressure Boiler Feed Water Pump	Liquid	Light brown color	Slight hydrocarbon odor

3.2.2 Methodology

An Olympus GX71 inverted microscope equipped with cross polarizers was used to detect liquid crystal domains in the samples. A camera, which was connected to the microscope, was used to record images. The detailed detection and observation procedure using cross-polarized light is reported in Chapter 2 and by Bagheri et al. [51]. Samples were spread on glass slides using syringes and then placed on the microscope stage. A series of photos was captured under both normal light and cross polarized light while water in the samples evaporated at room temperature, atmospheric pressure and ~33% humidity. Further analysis of the photos was conducted using software provided by Olympus. If present, liquid crystal domains appeared as bright, typically red, objects possessing a Maltese cross light pattern under cross-polarized light. Isotropic liquid, if present, appears dark under cross-polarized light.

3.3 Results and Discussion

3.3.1 Shell Peace River Bitumen Emulsion

Liquid crystal domains are present in the Shell Peace River bitumen emulsion (sample E). Maltese crosses are clearly visible in the sample as shown in Figures 3-3(a and b). The liquid crystals are identical in appearance to liquid crystals found in both hydrocarbons and laboratory based extracted-water-rich samples. Their diameter ~3 µm is similar to the size observed during laboratory extraction experiments (diameters ranging from 2.6 µm to 6 µm) but small relative to liquid crystals found in Athabasca bitumen fractions (diameters ranging from 10 µm in C_5 asphaltenes to ~50 µm in C_5 maltenes). The liquid crystal domains in this sample concentrated at the rim of water drops at the interface with the glass slide during water evaporation, as seen in Figure 3-3 (b). This phenomenon, known as the “coffee ring effect”, has been studied as an innovative and low-cost separation and concentration technology [52, 53]. After the water evaporated, the liquid crystal domains lost their shell structure and coalesced to form a film in the water free residue, Figure 3-3(d).

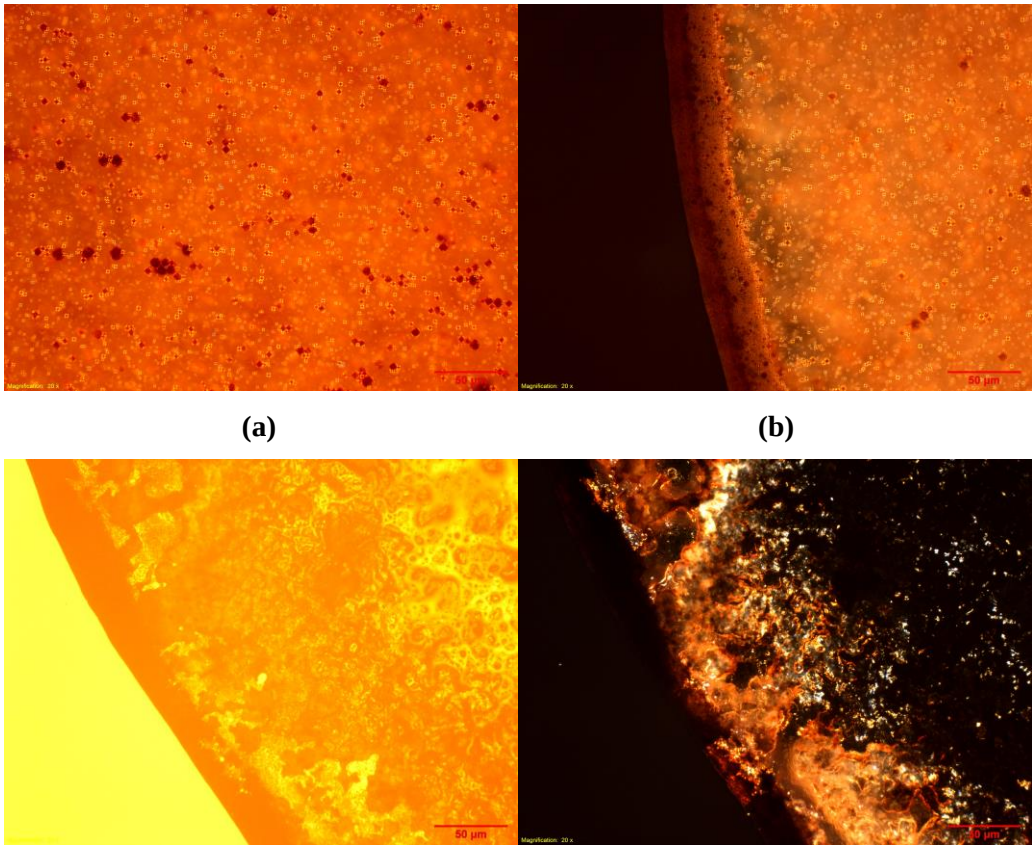

(a) **(b)**

(c) **(d)**

Figure 3-3 Microscopic observations of Shell Peace River bitumen emulsion (sample E) at 20x magnification: (a) central area of the sample under cross polarized light; (b) rim area of the sample under cross polarized light; (c) water free residue under normal light; (d) water free residue under cross polarized light.

3.3.2 Nexen FWKO Produced Water Samples

The Nexen samples comprise Produced Water from the Parallel Free-Water Knock-Out Drums A, B, C respectively. Since they all originated from the same initial emulsion, the discussion here is based on sample A. Samples B and C are the same as A. Figures 3-4(a and b) show microscopic observations of the Nexen FWKO drum water sample A. Few liquid crystals are present in the sample and their diameter is ~ 3 µm. For this case, the liquid crystals remained randomly dispersed on the glass slide in the residue following water evaporation, Figure 3-4(c and d).

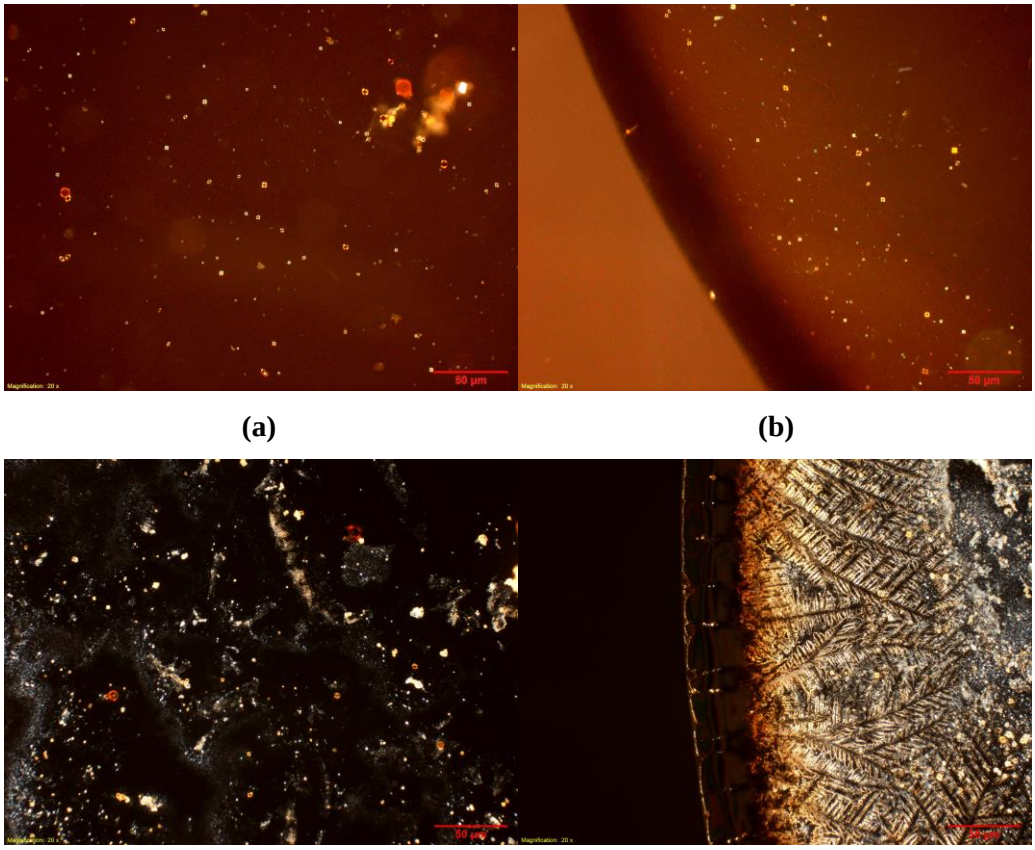

(a) **(b)**

(c) **(d)**

Figure 3-4 Microscopic observations of Nexen FWKO produced water sample A, at 20x magnification: (a) central area under cross polarized light; (b) rim area under cross polarized light; (c) central area of the water free residue under cross polarized light; (d) rim area of the water free residue under cross polarized light.

3.3.3 Flocculation in Nexen FWKO Produced Water Samples on Aging

Subsamples of the Nexen FWKO drum water samples (from samples A, B, and C), were allowed to stand for ~ 10 days in sealed containers at room temperature. Flocs appeared at the bottom of the vials in all three subsamples as illustrated in Figure 3-5. The flocs are visible in the sample, Figure 3-5(a), but are more clearly visible in the side and top views of the decanted subsamples, Figures 3-5(b and c). The flocs comprise organic materials, and are dark in color. The flocs were observed under both normal and cross-polarized light, as shown in Figure 3-6 (a-d). The flocs include microscopic liquid crystals with the average diameter ~3 µm. Dried flocs obtained from the decanted subsample, Figure 3-7, exhibit the coffee ring effect and liquid crystals remain present as shown in Figure 3-8 (a-d), where it is clear that the liquid crystals comprise the majority of the flocs.

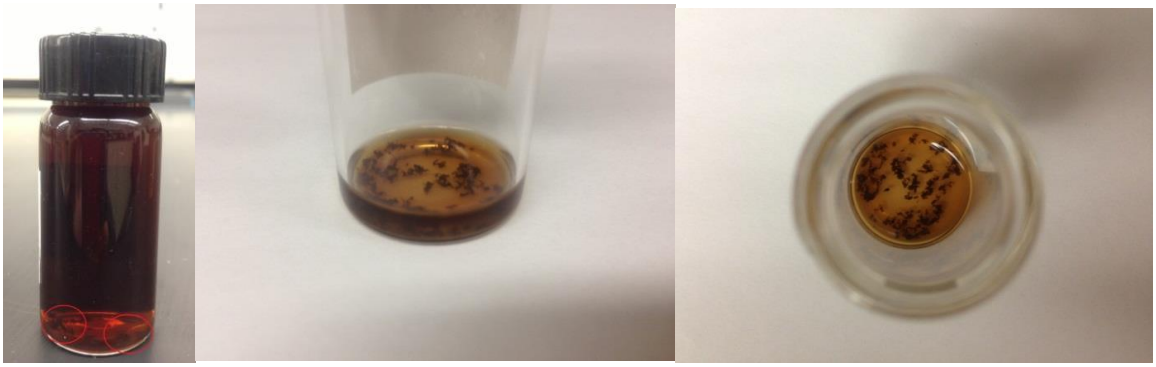

(a) **(b)** **(c)**

Figure 3-5 Aged Nexen FWKO produced water subsample A: a) red circles highlight visible flocs accumulated at the bottom of the vial, b) side and c) top view of flocs in the decanted sample.

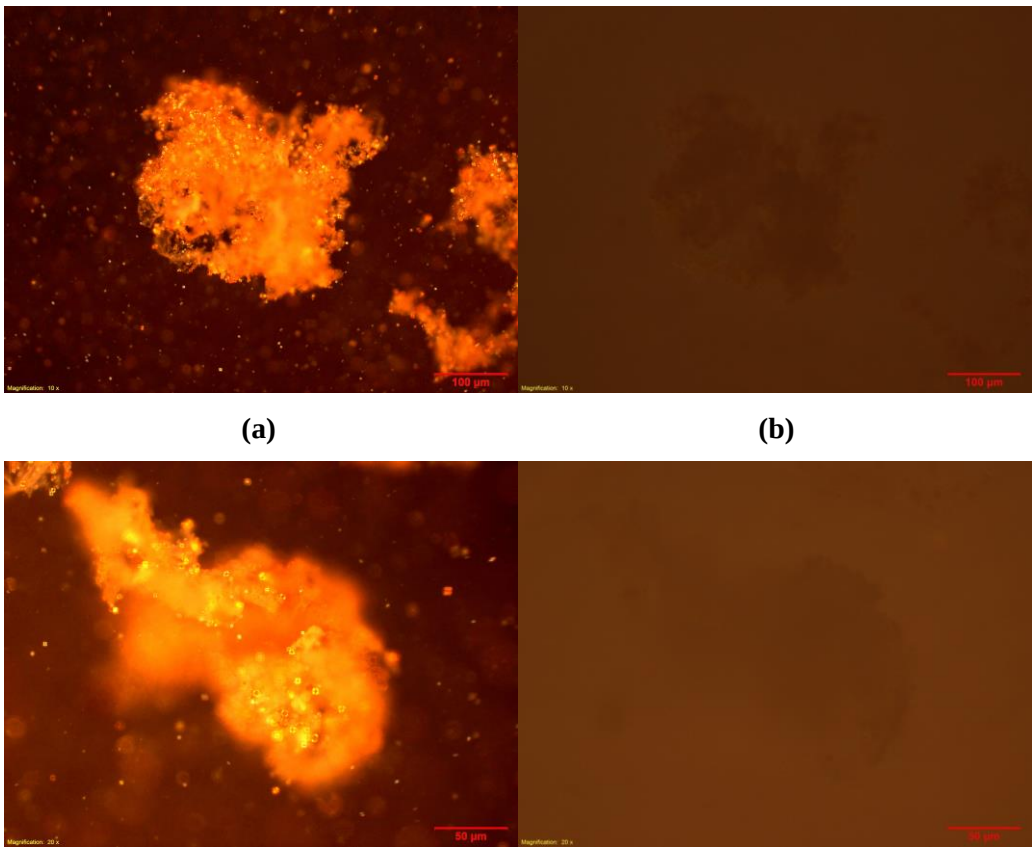

(a) **(b)**

(c) **(d)**

Figure 3-6 Microscopic observation of flocs in the aged Nexen FWKO subsample A:(a) under cross polarized light, magnification 10x; (b) under normal light, magnification 10x; (c) under cross polarized light, magnification 20x; (d) under normal light, magnification 20x.

Figure 3-7 Dried flocs from the aged Nexen FWKO subsample A.

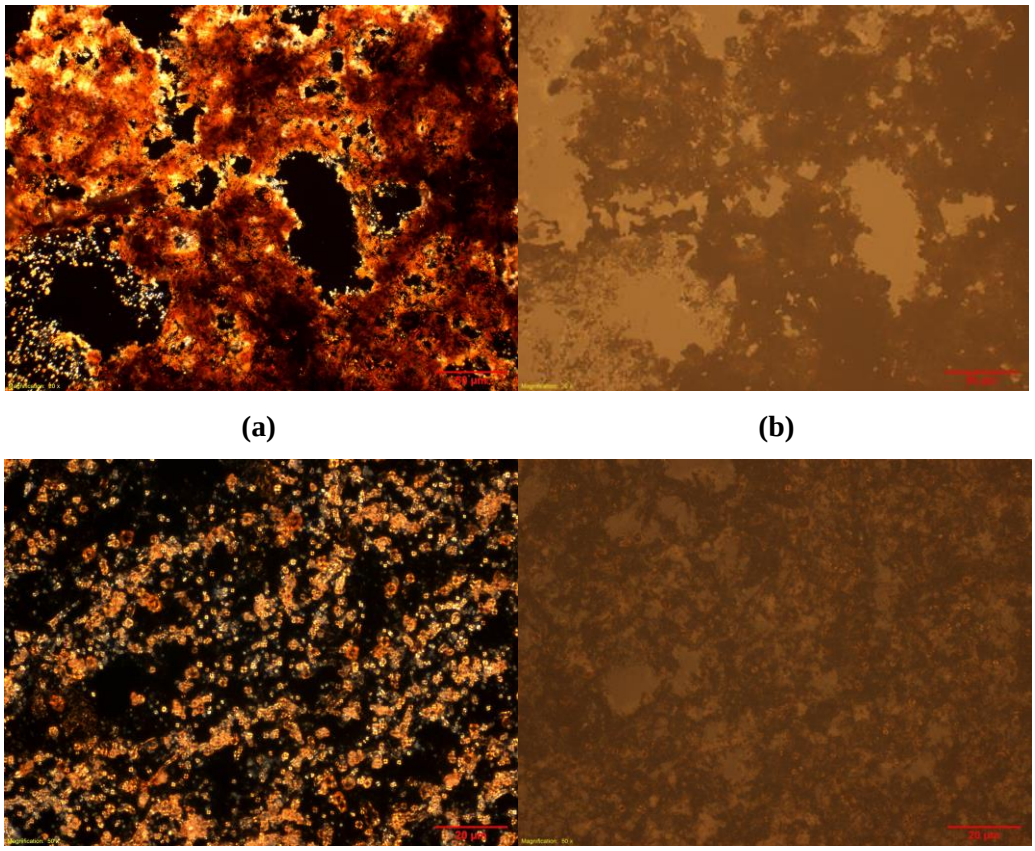

(a) **(b)**

(c) **(d)**

Figure 3-8 Microscopic observation of dried flocs from the aged Nexen FWKO subsample A: (a) under cross polarized light, magnification 20x; (b) under normal light, magnification 20x; (c) under cross polarized light, magnification 50x; (d) under normal light, magnification 50x.

3.3.4 Samples from Shell Orion (sample D) and ConocoPhillips Surmont (sample F)

The Shell Orion bitumen decanted water sample was obtained ten years ago and the precise sampling point is currently unavailable. Liquid crystals were not observed in this sample, Figure 3-9 (a), or in the water-free residue, Figure 3-9 (b). The ConocoPhillips Surmont sample, obtained from the low-pressure pump at the Once Through Steam Generator, revealed the same negative result - Figure 3-9 (c) and Figure 3-9 (d) for the sample and water free residue, respectively. Some additional objects appeared in the water free residue under the cross-polarized light, shown in Figure 3-9 (d). They are expected to be salt particles crystalized from the produced water, but they require additional analysis. To meet the zero liquid disposal criteria, all of the treated water (around 95% of the flow) accompanied by make-up water is pumped into the once through steam generator. At this step, the sample from ConocoPhillips reveals that the liquid crystals have been removed on or before the final water treatment step.

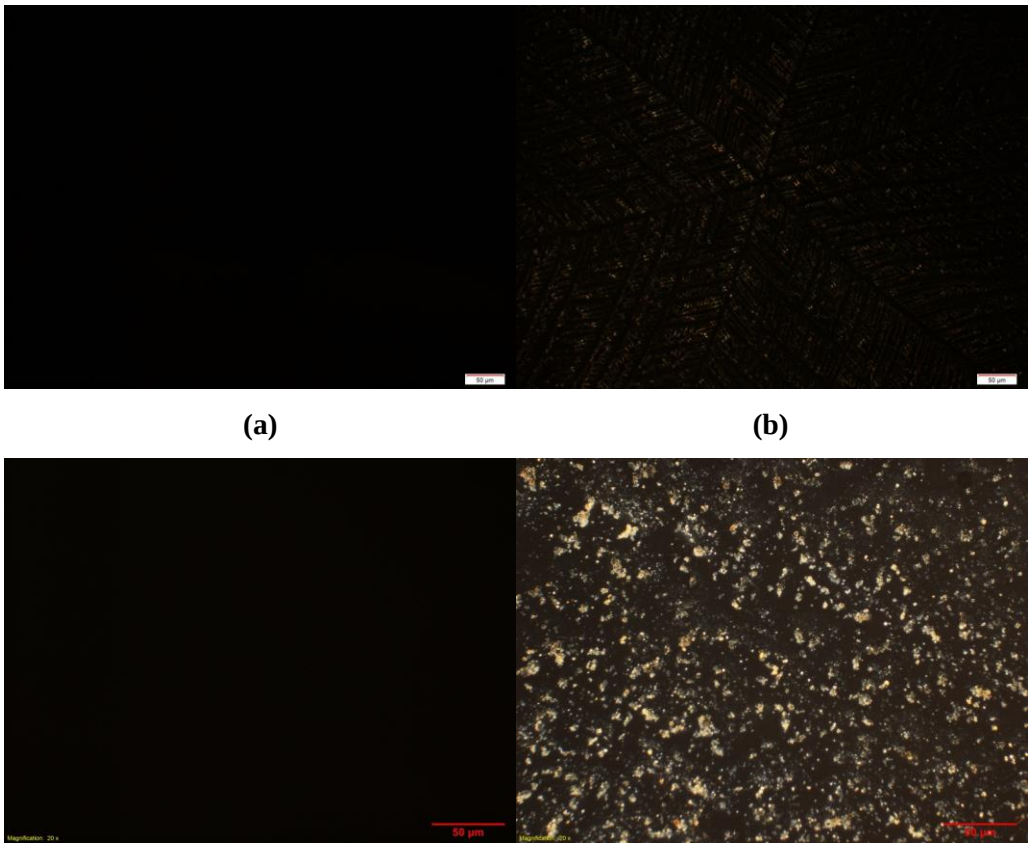

(a) **(b)**

(c) **(d)**

Figure 3-9 Microscopic observation of the Shell Orion and ConocoPhillips Surmont samples at 20x magnification:(a) Shell Orion sample under cross polarized light; (b) Shell Orion sample water-free residue under cross polarized light; (c) ConocoPhillips Surmont sample under cross polarized light; (d) ConocoPhillips Surmont sample water-free residue under cross polarized light.

3.3.5 Result Interpretation

Samples A-F were from different sampling points in different SAGD facilities. Each facility uses a specific process design and operating procedure for steam generation, water treatment, chemical addition, and water recycling. For example, the Nexen Long Lake SAGD facility uses five oil removal filters with Walnut shell media as the secondary de-oiling process followed by conventional water treatments (HLS and WAC processes, which makes the final Total Dissolved Solids (TDS) less than 0.20 ppm [27]), while Shell Orion uses induced static flotation along with an oil removal filter as the secondary de-oiling process. For water treatment, a de-aerator, evaporator and vapour separator are used there [26]. Despite such differences, the samples can be treated to a first approximation as if they were obtained from an integrated SAGD facility, Figure 3-2. Thus the produced

emulsion sample, sample E, comprises a high concentration of liquid crystals. It appeared that most, but not all, of the liquid crystals are eliminated during primary separation, as the water effluent from primary separation, samples A, B and C, have much lower liquid crystal contents. Diluents or demulsifiers are usually added into the emulsion before or during the preliminary separation process. This raises questions concerning the nature of the "recapture mechanism" (whether the liquid crystals are broken and dissolved into the oil, or whether the liquid crystals are physically redispersed in the oil phase) and whether the treatments currently employed are optimal. The boiler feed water sample, sample F, confirms that liquid crystals can be eliminated during de-oiling and water treatment processes – at least in one case.

3.4 Summary and Future Works

This field study confirms the key result of the laboratory-based study in chapter 2. A fraction of organic liquid crystals present initially in bitumen are transferred from the bitumen phase to the water phase during SAGD production.

The liquid crystals transferred to the water phase, possessing diameters of ~ 3 microns, are one order of magnitude smaller in size than the average size of liquid crystals in fractions of Athabasca bitumen.

Most but not all of the liquid crystals transferred to the water phase are returned to the bitumen phase during primary separation. Liquid crystal domains are absent from the boiler feed water sample, indicating that the residual liquid crystals are captured by secondary separation or subsequent water treatment processes.

The capture mechanisms and physical state of the liquid crystals on capture are both unknown but are likely to vary with the details of the water treatment processes employed. Three types of research are warranted as time, opportunity and budgets permit.

1. Follow-up studies examining the fate of liquid crystals in specific SAGD surface facilities. Emulsion/water samples before and following each stage of water

treatment are required. These applied studies require close collaboration with one or more of the sponsoring companies. The objective is to identify the best practices.

2. Liquid crystal recapture mechanisms should be analyzed. Liquid crystal recapture is likely to be mechanistically different from liquid drop transfer, and is likely to vary with process details.
3. The desirability and feasibility of separating liquid crystals as a by-product from SAGD surface facilities is worth exploring.

Chapter 4 Growth of Liquid Crystal Films

4.1 Introduction

Colloid science has become of great importance for industrial applications and daily life, from coating, to paints and inks, to medicine, and to food processing and environmental protection[54]. One interesting phenomenon related to colloid science is the following: when a drop of a particle suspension is dried on a solid surface, the particles move to the periphery and deposit in the form of a ring, the well-known coffee ring effect [55]. A lot of research has been conducted to understand the mechanism of the ring formation, for example, with the use of micron-sized polystyrene particle dispersions [56-59]. This effect could potentially be applied as an innovative and simple separation technology [52].

From Chapters 2 and 3, the transfer of liquid crystals from the bitumen to water-rich phase does happen in both laboratory scale and industrial SAGD facilities even though the transfer mechanism remains unknown. Separation and enrichment of the liquid crystal domains has become another interesting research tasks. In this chapter, the growth behavior of liquid crystals upon drying of sessile water-rich sample droplets is studied. If the models related to the drying process in the polystyrene suspensions apply, two factors can be considered: the concentration of liquid crystal rich domains and the diameter of the sessile drops. The goal is to manipulate and maximize the accumulation at the rim so that the liquid crystal rich domains can be separated and enrich liquid crystal domain samples can be obtained for further compositional analysis such as XPS and FT-ICR [60].

4.2 General Theory

Basically, three stages are involved in the process of drying colloidal dispersions by evaporation of the liquid medium [61]: drying stage, particle deformation stage, and coalescence + molecular diffusion across the particle boundaries stage.

Drying Stage: The coffee ring effect dominates during the drying process. While the water evaporates, the contact line of a sessile droplet remains fixed, and the loss of water leads only to the contact angle decrease (β1>β2>β3), as illustrated in Figure 4-1. The outward capillary flow, induced by the evaporation, carry the liquid crystals from the drop center to the surface, and the liquid crystals become concentrated in the rim area of the drop. The analytical expression for the outward radial flow velocity V_{rad} could scales as $V_{rad} \sim j/r$, where j is the evaporation mass flux and ρ is the density of drop liquid. At the end of this stage, the liquid crystals become closer to each other, eventually touching to form a loose pack. Compaction and deformation does not occur [57].

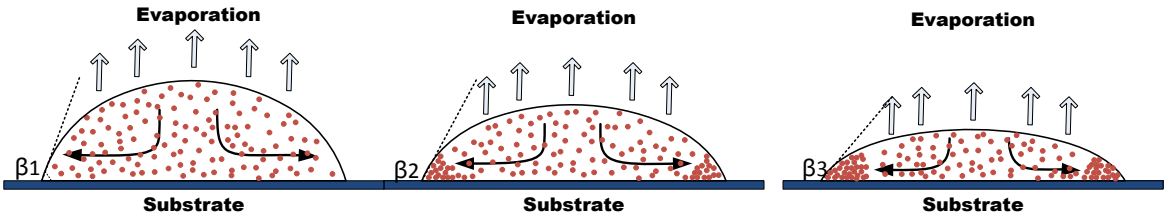

Figure 4-1 The liquid crystals in the water phase tend to accumulate at the rim area of the sessile drop.

However, If a drop is placed on a heated substrate, inefficient heat transfer through the drop introduces a temperature gradient, which leads to an upward flow along the curvature of the droplet from the substrate contact region of lowest surface tension (high temperature) to the apex surface region of highest surface tension (low temperature). This is known as the Marangoni flow effect. It opposes the radial convective flow and together with the outward radial flow forms the circulation flow loop illustrated in Figure 4-2. Adding a surfactant [62] or altering the evaporation to the surroundings [63] affect the rate the Marangoni flow.

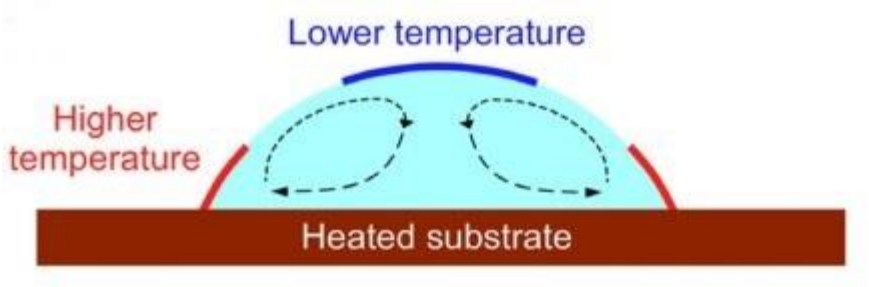

Figure 4-2 A Marangoni flow pattern in an evaporating drop on a heated substrate [64]

For the heated substrate case, the Marangoni recirculation flow velocity V_{Ma} may scale as $V_{Ma} \sim (1/32)\left(bf^2 \mathrm{D}T/m\right)$, where the ϕ is the wetting angle of the drop, μ is the dynamic viscosity, β is the gradient of surface tension with respect to the temperature, and ΔT is the temperature difference between the edge and the apex of the droplet [65].

The flow will counter the radially outward flow [65] and the deposition pattern is controlled by the competition between these two convective flow patterns. For cases where Marangoni convection dominates over the radially outward flow, the deposition pattern will be a central bump or a uniform deposition over the entire wetting area, while in a system where the Marangoni convective flow is negligible compared to radial flow, a ring deposition pattern is observed [66].

In the following experimental section, a drop comprising a liquid crystal dispersion is placed on a substrate and exposed to ambient conditions. As the temperature gradient is negligible, Marangoni flow plays may be ignored. Outward radial flow dominates and ring deposition occurs.

To a simple approach, a dimensionless number C_R was introduced for the quantitative measure of the successful ring structure formation [53]:

$$C_R = \frac{\tau_{\text{particle}}}{\tau_{\text{evap}}},$$

where τ_{particle} is the time that allows the adjacent particles to meet each other at the rim area, and τ_{evap} is the evaporation time of the drop.

The coffee ring forms when $C_R << 1$ while no coffee ring forms when $C_R > 1$ [53].

So in order to have the coffee ring effect, we need to increase τ_{evap} while decreasing τ_{particle} as much as possible.

Based on the constant contact diameter evaporation model proposed by Popov [67], the time scale of evaporation can be expressed as:

$$\tau_{evap} = \frac{\theta_{initial} - \theta_{receding}}{4K} \pi \left(\frac{D}{2} \right)^2 ,$$

Where K is a parameter representing the drop evaporation rate, D is the diameter of the drop, $\theta_{initial}$ and $\theta_{receding}$ represent the initial contact angle and receding contact angle respectively.

The τ_{particle} value can be expressed in the form of the Einstein diffusion equation:

$$\tau_{particle} = \frac{\overline{L_m^2}}{2D_p} = \frac{\left(\sqrt[3]{V_d / n} \right)^2}{2D_p},$$

where $\overline{L_m}$ is the mean distance between two adjacent particles within the liquid drop and can be estimated as $\overline{L_m} = \sqrt[3]{V_d / n}$, V_d is the volume of the drop and n is the number of dispersed particles in the drop. V_d / n can be interpreted as the reciprocal of the liquid crystal domain concentration in water phase, D_p is the diffusion constant of the particle in a low viscosity liquid medium which can be treated as a constant in a specific liquid medium [1].

To simplify the approach, one can assume that the observation temperature, relative humidity, volatility of the solvent, the medium and the size of the liquid crystals are fixed, so the evaporating rate is a constant. The concentration of the liquid crystal domains and the diameter of a drop become two important factors for evaluating C_R :

$$C_R = \frac{\tau_{\text{particle}}}{\tau_{\text{evap}}} = \frac{\dfrac{\left(\sqrt[3]{V_d / n} \right)^2}{2D_p}}{\dfrac{\left(\theta_{initial} - \theta_{receding} \right)}{4K} \pi \left(\frac{D}{2} \right)^2} = \frac{8K}{\left(\theta_{initial} - \theta_{receding} \right) \pi D_p} \times \frac{1}{D^2} \times \frac{1}{\left(\sqrt[3]{n / V_d} \right)^2}$$

Larger concentrations of liquid crustal domains and larger drops promote the coffee ring effect.

The Particle Deformation Stage: At the final stage of the drying process, the packing of the particles becomes close without voids, where the interfacial tension is a driving force for particle deformation. This includes the air-water, water-particle or particle-air interfacial tension or surface adhesive forces in the dispersion system [68].

Coalescence and Molecular Diffusion Stage: When the particles are closely packed, they tend to coalesce with one another. The process is driven by a reduction in surface energy associated with the particle surface. As a result, a continuous film is formed. The formation of latex films at this stage has been thoroughly studied using polymer dispersions [69, 70].

4.3 Experimental Methods

4.3.1 Sample Preparation

Two samples were prepared for this study. The water-extraction sample shown in Figure 4-2 (a) is a liquid crystal–in-water sample prepared as described in Chapter 2. The second sample, a concentrated sample, shown in Figure 4-2 (b), was obtained from the sample shown in Figure 4-2 (a) by evaporating ~ 50 % of the water present using a Fischer Scientific Isotemp Oven at 70°C overnight. The micro scale view (Figure 4-3) also illustrates that the concentration of liquid crystals in the concentrated sample is much higher than in the original one. Although the exact concentration is not known, this qualitative estimation of concentration can be used as a parameter for comparison.

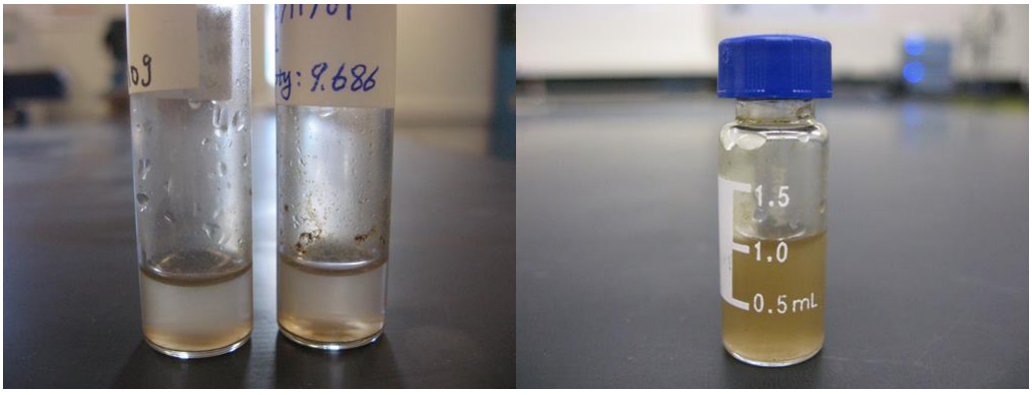

(a) **(b)**

Figure 4-3 Bulk view of the (a) original sample and (b) concentrated sample.

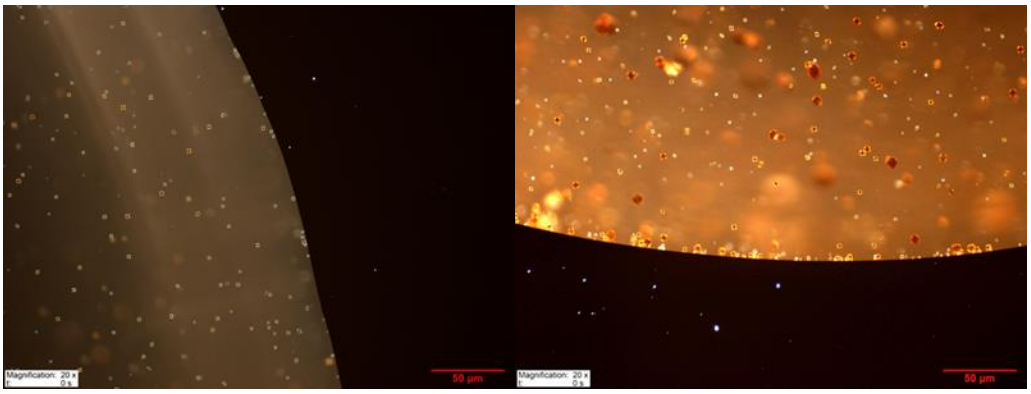

(a) **(b)**

Figure 4-4 The microscopic view of (a) the liquid crystal sample and (b) the concentrated liquid crystal concentrated sample. (Scale bars are 50 μm).

4.3.2 Confocal Cross Polarized Light Microscopy

For each experiment, drops with different volume (10 μL, 30 μL and 50 μL) were placed on a microscope slide, which had been pre-cleaned with methanol to remove dust and grease. The drops were loaded on to the slide by a Hamilton 100 μL micro syringe. Then the slide was placed on the observation stage of the microscope and the drop was left to evaporate at 25^{o}C, atmospheric pressure and ~33% humidity. Cross-polarized light in situ observation was conducted for recording the movement of the liquid crystal domains to the rim area of the sessile drops.

4.4 Results and Discussion

4.4.1 Low Concentration Drops

Figure 4-4, Figure 4-5 and Figure 4-6 comprise a series of images captured upon evaporation of low concentration sessile drops with the volumes of 10 μL (diameter is ~0.45cm), 30 μL (diameter is ~0.60cm) and 50 μL (diameter is ~0.75cm), respectively, indicating the drying stage and the final deposit shape of liquid crystal domains. It is evident that the liquid crystal domains tend to accumulate at the water-air interface and a relatively large number of them move to the rim to form a ring-like profile after the water has evaporated, although many particles are dispersed randomly as well.

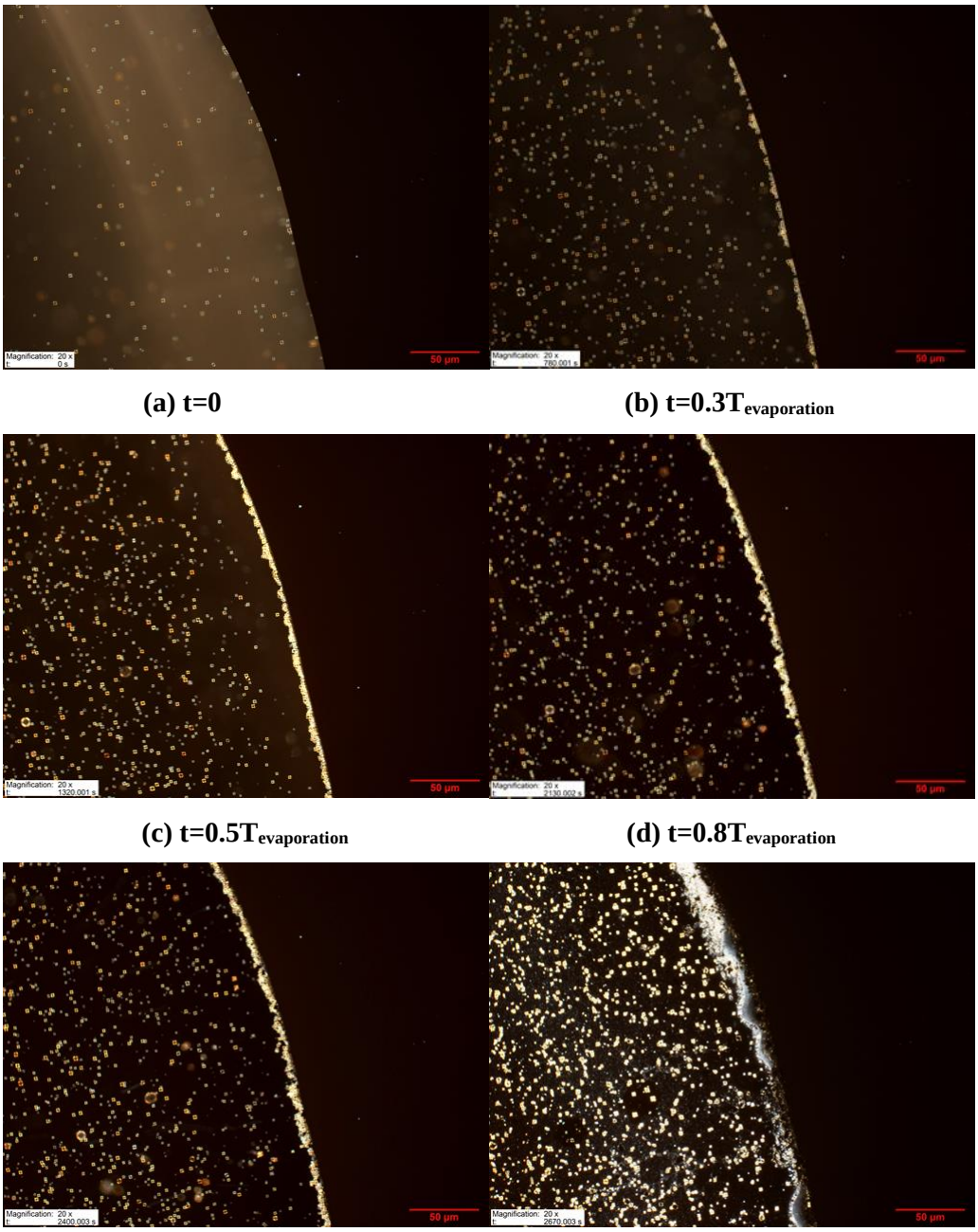

(a) t=0 **(b) t=0.3$T_{evaporation}$**

(c) t=0.5$T_{evaporation}$ **(d) t=0.8$T_{evaporation}$**

(e) t=0.9$T_{evaporation}$ **(f) t=1.0$T_{evaporation}$**

Figure 4-5 A series of images illustrating the growth of liquid crystals at the rim area in a 10 µL sessile drop of the low concentration sample.t is the fraction of the total evaporation time $T_{evaporation}$ = 2670 seconds for the sessile drop.

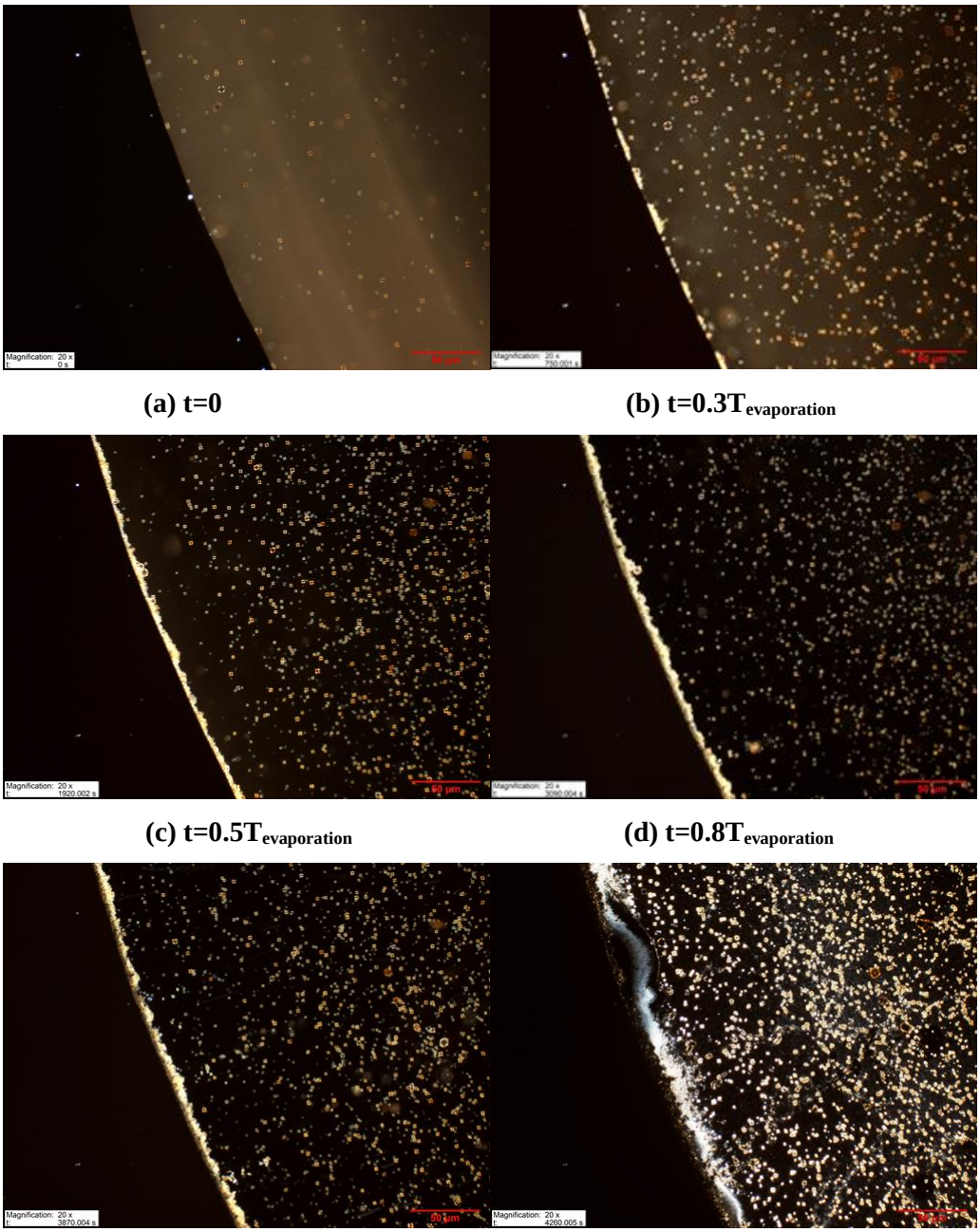

(a) t=0 **(b) t=0.3$T_{evaporation}$**

(c) t=0.5$T_{evaporation}$ **(d) t=0.8$T_{evaporation}$**

(e) t=0.9$T_{evaporation}$ **(f) t=1.0$T_{evaporation}$**

Figure 4-6 A series of images illustrating the growth of liquid crystal domains at the rim area in a 30 µL sessile drop of the low concentration sample. t is the fraction of the total evaporation time $T_{evaporation}$ = 4260 seconds for the sessile drop.

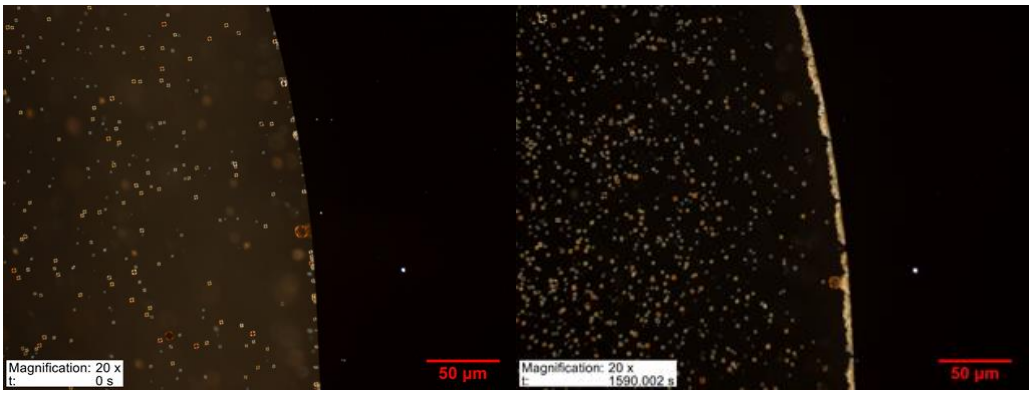

(a) t=0 **(b) t=0.3$T_{evaporation}$**

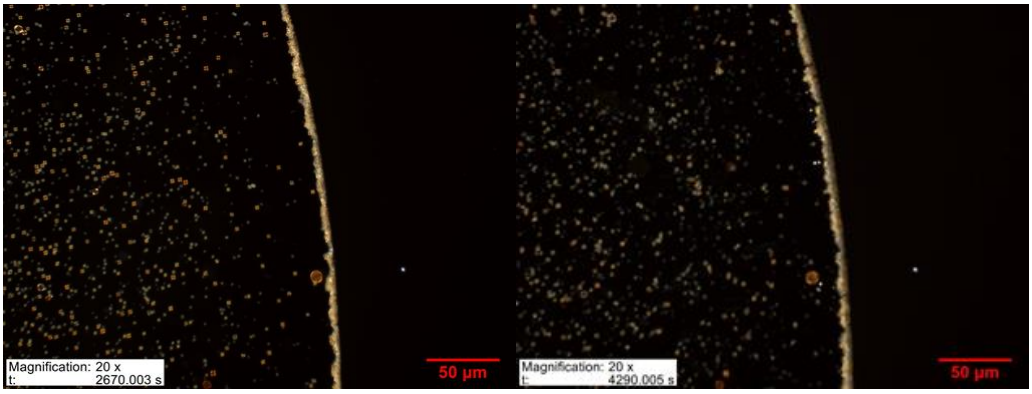

(c) t=0.5$T_{evaporation}$ **(d) t=0.8$T_{evaporation}$**

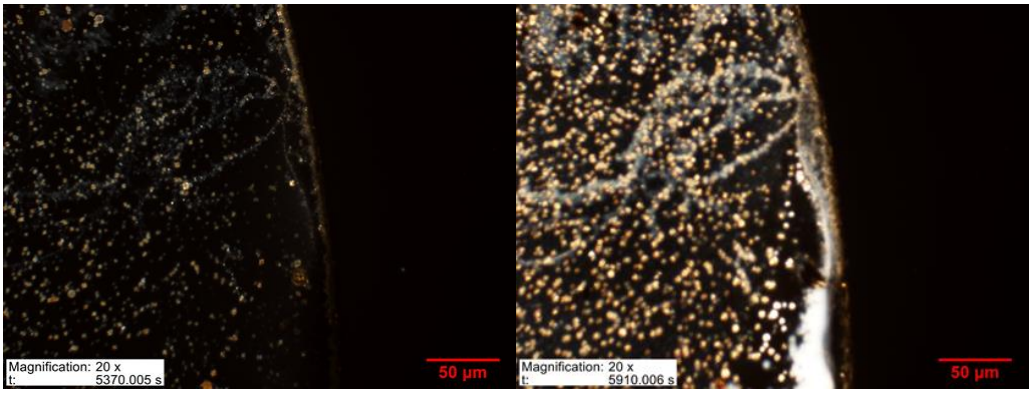

(e) t=0.9$T_{evaporation}$ **(f) t=1.0$T_{evaporation}$**

Figure 4-7 A series of images illustrating the growth of liquid crystal domains in the rim area in a 50 µL sessile drop of the low concentration sample. t is the fraction of the total evaporation time $T_{evaporation}$ = 5910 seconds for the sessile drop.

However, the variation of the diameter of the sessile drop from 0.45 cm to 0.75cm did not lead to an observable intensification of the coffee ring effect. As shown in Figure 4-7, the thicknesses of the liquid crystal domains that accumulate in the rim area ~ 10 μm is independent of sessile drop diameter during the drying processes.

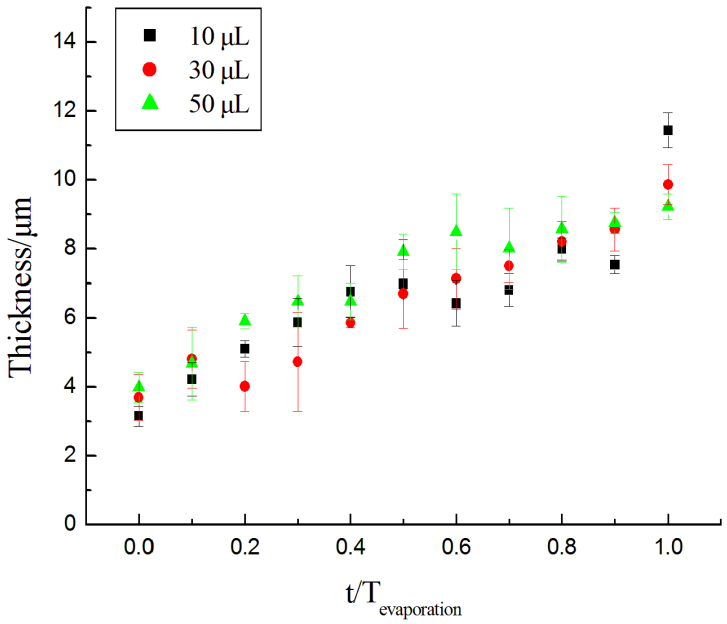

Figure 4-8 Liquid crystal ring thickness during the drying process for the low concentration samples.

4.4.2 Concentrated Samples

Figure 4-8, Figure 4-9 and Figure 4-10 are the time sequence images captured upon evaporation of the concentrated sessile drop samples. The drop volumes are 10 μL (diameter is ~0.45cm), 30 μL (diameter is ~0.60cm) and 50 μL (diameter is~0.75cm) respectively. As with the low concentration sample, the liquid crystals also accumulated and formed a ring in the rim area driven by the coffee ring effect. Since the concentration of the concentrated sample is higher than that of the original sample, the effect is intensified.

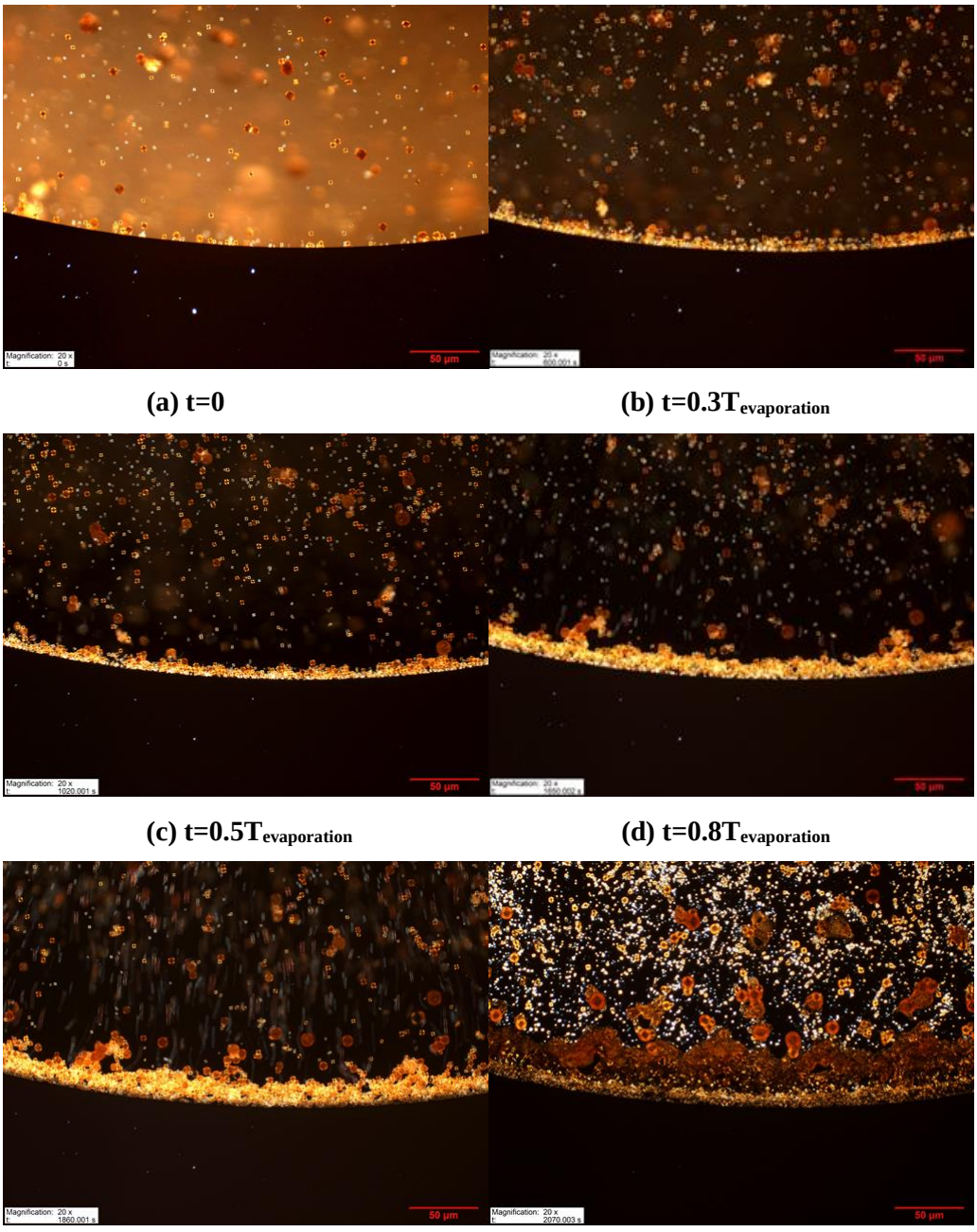

(a) t=0 **(b) t=0.3$T_{evaporation}$**

(c) t=0.5$T_{evaporation}$ **(d) t=0.8$T_{evaporation}$**

(e) t=0.9$T_{evaporation}$ **(f) t=1.0$T_{evaporation}$**

Figure 4-9 A series of images illustrating the growth of liquid crystals in the rim area of a 10 µL sessile drop of the concentrated sample. t is the fraction of the total evaporation time $T_{evaporation}$ = 2070 seconds for the sessile drop.

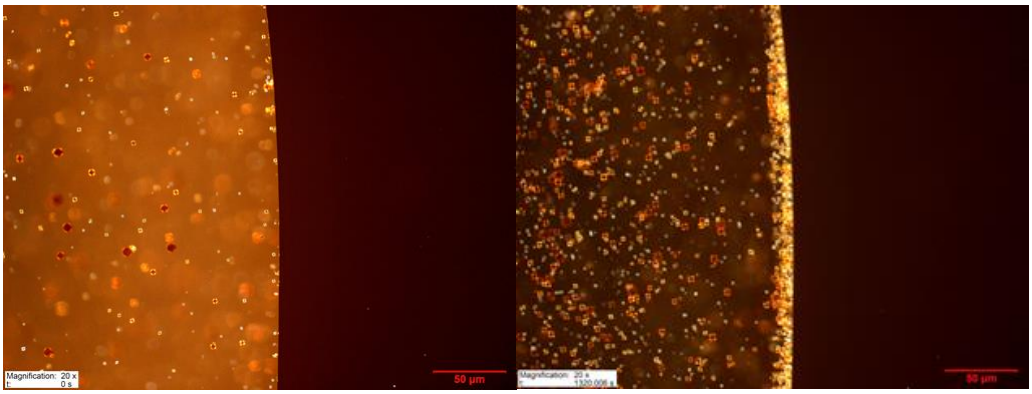

(a) t=0 **(b) t=0.3$T_{evaporation}$**

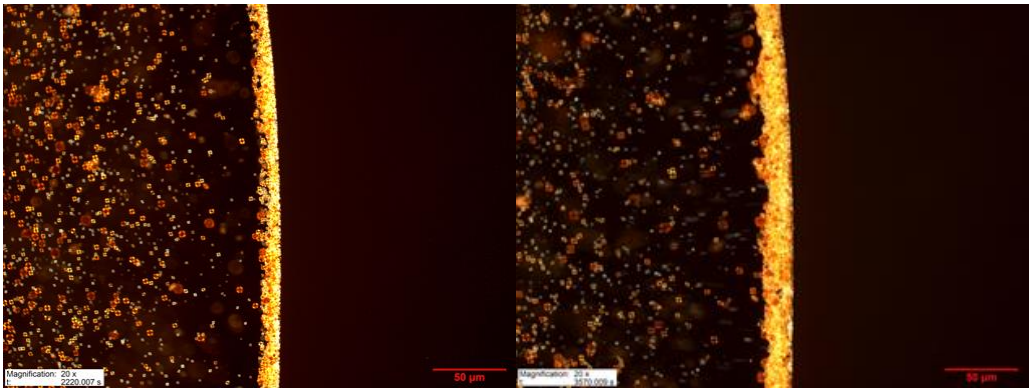

(c) t=0.5$T_{evaporation}$ **(d) t=0.8$T_{evaporation}$**

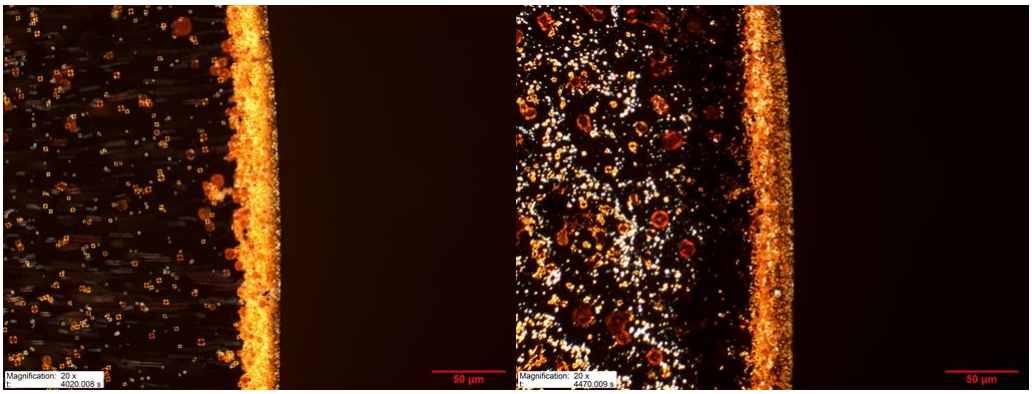

(e) t=0.9$T_{evaporation}$ **(f) t=1.0$T_{evaporation}$**

Figure 4-10 A Series of images illustrating the growth of liquid crystals in the rim area of a 30 µL sessile drop of concentrated sample. t is the fraction of the total evaporation time $T_{evaporation}$ = 4470 seconds for the sessile drop.

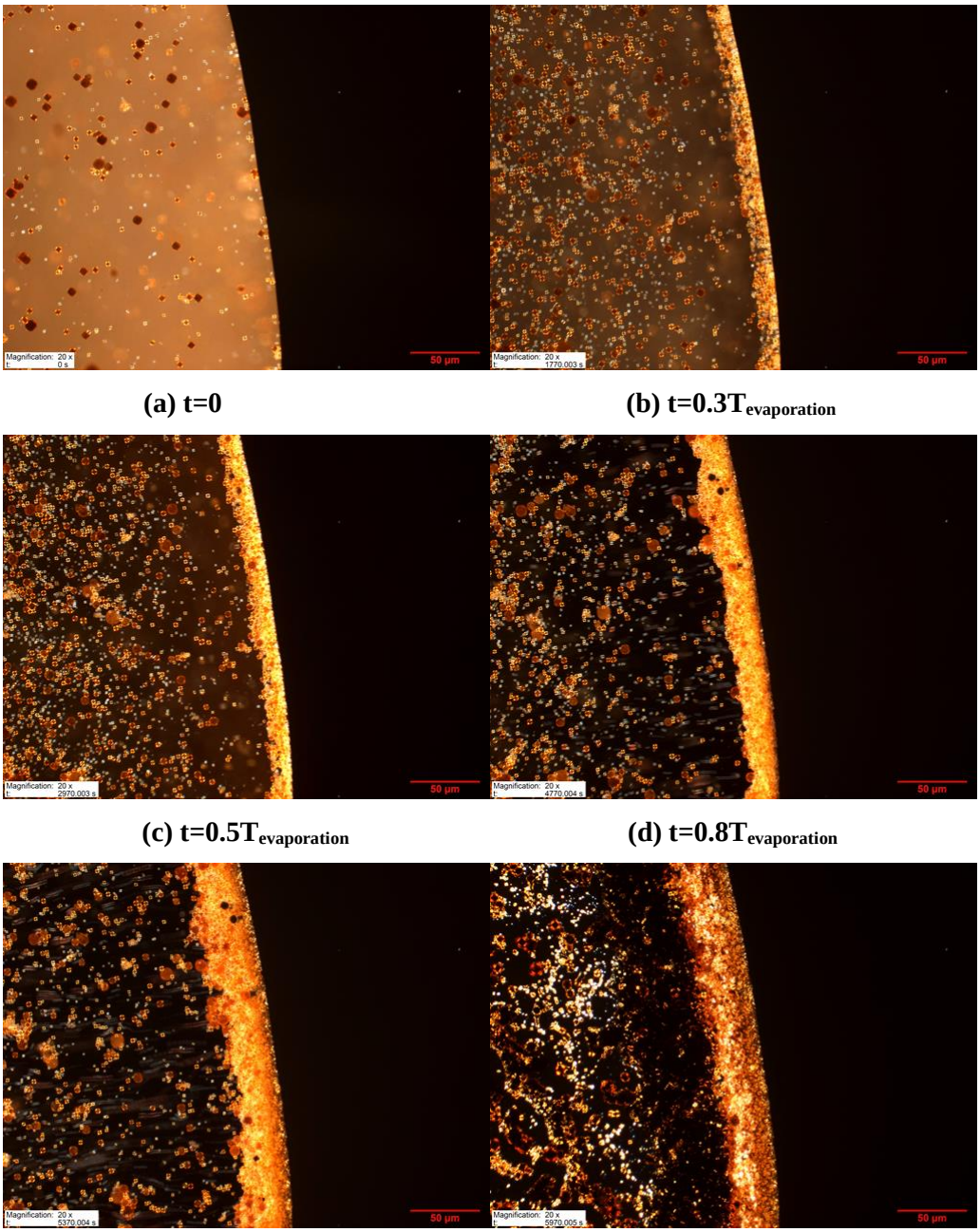

(a) t=0 **(b) t=0.3$T_{evaporation}$**

(c) t=0.5$T_{evaporation}$ **(d) t=0.8$T_{evaporation}$**

(e) t=0.9$T_{evaporation}$ **(f) t=1.0$T_{evaporation}$**

Figure 4-11 A series of images illustrating the growth of liquid crystal domains in the rim area of a 50 µL sessile drop of concentrated sample. t is the fraction of the total evaporation time $T_{evaporation}$ = 5970 seconds for the sessile drop.

The coffee ring effect is more intense in at higher concentration. Figure 4-11 shows the time dependent ring thicknesses for sessile drops with different diameters. The thickness reached 45 µm for larger drops.

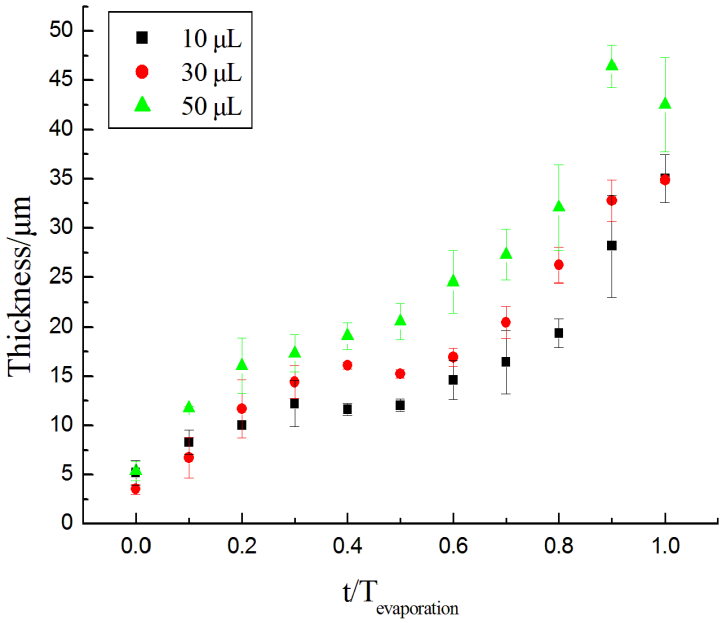

Figure 4-12 The accumulating thickness of liquid crystal domains during the drying process for high concentrations drops.

Table 4-1 shows a summary of the observations. The concentration of liquid crystal domains is the primary factor and the diameter of the sessile drops has a minor impact on the intensity of the coffee ring. In order to get more liquid crystal domains to accumulate in the rim area, the extracted sample must be concentrated first, and then placed on a glass slide for free evaporation.

Table 4-1 Summary of the experimental observations

Sample Type	Average Size of Liquid Crystal	Concentration	Volume (Diameter)	Final Thickness (water evaporated)	Coffee Ring Effect
low concentration Extracted Liquid	~4 μm	Low	10 μL (~0.45cm)	11.43 μm	Negligible
			30 μL (~0.60cm)	9.86 μm	Negligible
			50 μL (~0.75cm)	9.22 μm	Negligible
More Concentrated Extracted Liquid	~4 μm	High	10 μL (~0.45cm)	35.01 μm	Significant
			30 μL (~0.60cm)	34.87 μm	Significant
			50 μL (~0.75cm)	44.67 μm	Significant

4.4.3 Liquid Crystal Deformation and Coalescence

With the low concentration samples, the liquid crystal film formed is thin, and it is hard to conduct in situ observations of the liquid crystal domain deformation stage and liquid crystal domain coalescence. For the high concentration samples, the thickness of the film formed is larger, so it is easier to observe these two stages. Figure 4-12 shows the final stages of the evaporation process for the 50 μL sessile condensed sample drop. It is clear that during the final period of the evaporation process (close to but smaller than $1.0T_{evaporation}$), the liquid crystal domains accumulated in the rim area form a close pack, but the boundaries between the liquid crystals remain visible. After the water has evaporated, the liquid crystal domains are deformed and coalesce to form a continuous film as shown in Figure 4-12 (b).

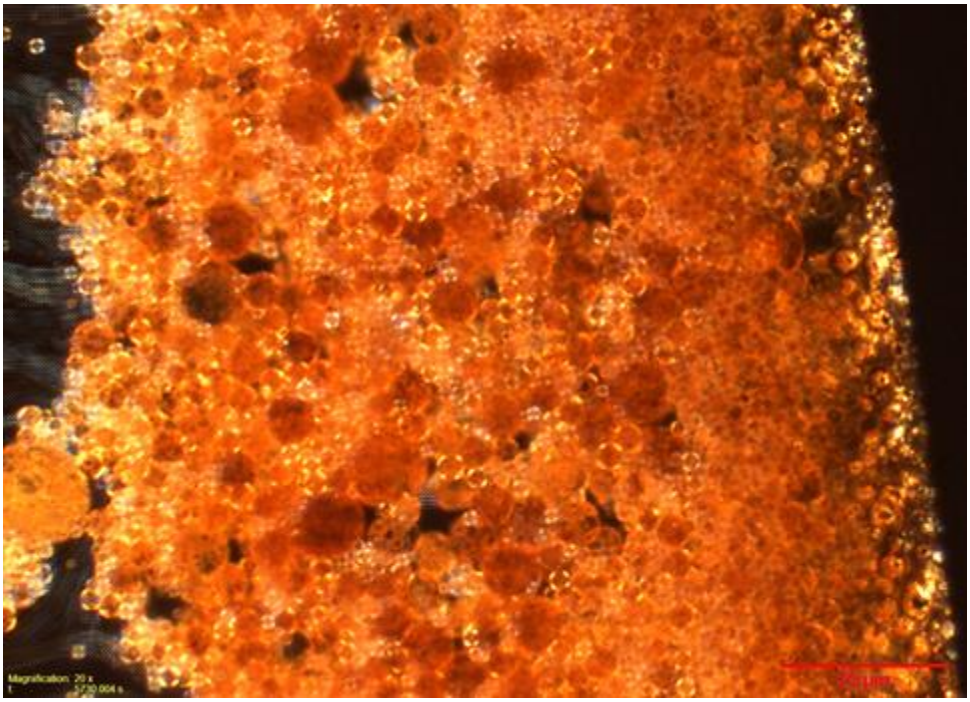

(a)

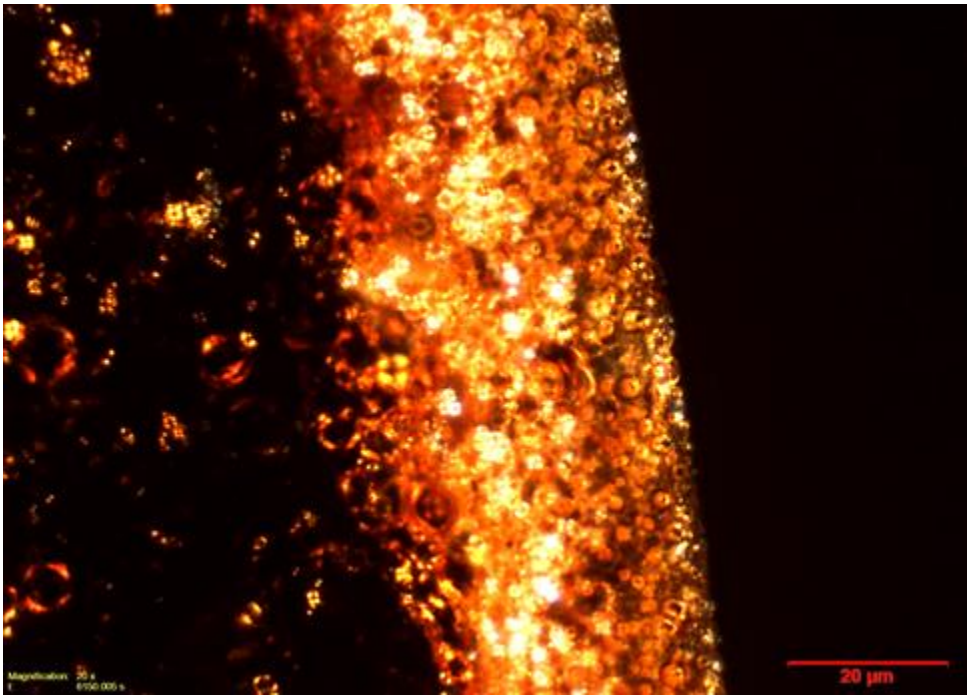

(b)

Figure 4-13 Final stages of the accumulation of liquid crystal domains in the rim area in a 50 µL sessile drop for a concentrated sample: (a) t is close to but smaller than $1.0T_{evaporation}$; (b) t> $T_{evaporation}$ (water evaporated). The scale bar is 20 µm.

4.5 Summary

1. The presented study confirms that liquid crystal domains in the water phase accumulate and form a ring like deposit similar to polymer colloid dispersions during the drying process. This offers an innovative way for liquid crystals separation and enrichment.
2. Liquid crystal concentration (primary variable) and sessile drop diameter (secondary variable) influenced the accumulation of liquid crystal domains in the rim area of a drying sessile drop.
3. Separation of the liquid crystal shell from the isotropic core remains an unsolved challenge.

Chapter 5 Conclusions and Future Work

5.1 Conclusions

Laboratory-scale experiments:

- The laboratory scale experiments show that liquid crystal domains transfer from the bitumen rich phase to the water-rich phase in water + Athabasca bitumen mixtures heated to in-situ production conditions (473 K, 523 K and 593 K, the pressures were 1.55 MPa, 3.97 MPa and 11.27 MPa respectively) and then cooled to room temperature.
- The structure of the liquid crystal domains transferred to the water rich phase are identical to those identified in the hydrocarbon-rich phases. The diameter of the liquid crystal domains in the water phase ranged from 2.4 μm to 5.6 μm, one order of magnitude smaller than those found in the hydrocarbon phase. They were more mobile in water phase and tended to concentrate at the rim of sessile drops of water, with the effect accentuated as water was evaporated.
- The transfer mechanism for liquid crystal domains from the bitumen-rich phase to the water-rich phase still remains unresolved.

SAGD Field Study:

- The field study confirmed that a fraction of organic liquid crystal domains present initially in bitumen are transferred from the bitumen-rich phase to the water-rich phase during SAGD production. These liquid crystal domains, which possess diameters of ~ 3 microns, are one order of magnitude smaller in size than the average size of liquid crystal domains in fractions of Athabasca bitumen.
- Most but not all of the liquid crystals transferred to the water-rich phase are returned to the bitumen-rich phase during primary separation in surface facilities. Liquid crystal domains are absent from the boiler feed water sample, indicating that the residual liquid crystal domains are captured by secondary separation or subsequent water treatment processes.

- The recapture mechanism and the physical state of the liquid crystal domains upon recapture by the bitumen-rich phase are unknown but are likely to vary with the details of the water treatment processes employed.

Growth of Liquid Crystal Films:

- The liquid crystal domains in the water-rich phase accumulate and form a ring like deposit similar to polymer colloid dispersions during the drying process. This offers an innovative way for liquid crystal domains to be separated and enriched.
- Two factors affect the ring structure formation in polymer dispersions: the liquid crystal domain concentration and the diameter of a sessile drop both affect the accumulation of liquid crystal domains at the rim of sessile drops. Concentration plays a primary role. In order to get a thick ring of liquid crystal film, low concentration samples should be concentrated.
- Separation of the liquid crystal shell from the isotropic core was not achieved.

5.2 Recommendations for Future Work

- Liquid crystal domain transfer and recapture mechanisms should be identified by laboratory scale in-situ observation.
- A follow-up study should be conducted based on a specific plant in order to identify the fate and transfer mechanisms related to liquid crystal domains in SAGD surface facilities. Such a study would require close collaboration with one or more of the sponsoring companies. The objective is to identify best practices.
- The desirability and feasibility of separating liquid crystals as a by-product from SAGD surface facilities is worth exploring.
- Isolated liquid crystals films from the water phase are recommended for compositional analysis such as XPS or FT-ICR.

References

1. Einstein, A., *Investigations on the Theory of the Brownian Movement*1956: DoverPublications. com.
2. Würflinger, A., *Dielectric studies under pressure on plastic and liquid crystals.* International Reviews in Physical Chemistry, 1993. **12**(1): p. 89-121.
3. Corcoran, J., et al., *Amphitropic liquid crystals. Part 1.-Effect of a thermotropic mesogen on lyotropic mesomorphism, and of a surfactant on thermotropic mesomorphism. The C16EO8-5-CB-water system.* Journal of Materials Chemistry, 1992. **2**(7): p. 695-702.
4. Brown, G.H. and W.G. Shaw, *The Mesomorphic State - Liquid Crystals.* Chemical Reviews, 1957. **57**(6): p. 1049-1157.
5. Syrbu, S., R.Y. Golovanov, and V. Klopov, *Properties of Some Mesogens in the Liquid Crystal and Isotropic States.* Theoretical Foundations of Chemical Engineering, 2003. **37**(2): p. 204-206.
6. van der Kooij, F.M., K. Kassapidou, and H.N. Lekkerkerker, *Liquid crystal phase transitions in suspensions of polydisperse plate-like particles.* Nature, 2000. **406**(6798): p. 868-871.
7. Bagheri, S.R., et al., *Physical Properties of Liquid Crystals in Athabasca Bitumen Fractions.* Energy & Fuels, 2012. **26**(8): p. 4978-4987.
8. Bagheri, S.R., et al., *Observation of Liquid Crystals in Heavy Petroleum Fractions.* Energy & Fuels, 2010. **24**(8): p. 4327-4332.
9. Masik, B.K., *Separation and analysis of liquid crystalline material from heavy petroleum fractions*, in *Department of Chemical and Materials Engineering*2011, University of Alberta: Edmonton.
10. McKenna, A.M., et al., *Identification of Vanadyl Porphyrins in a Heavy Crude Oil and Raw Asphaltene by Atmospheric Pressure Photoionization Fourier Transform Ion Cyclotron Resonance (FT-ICR) Mass Spectrometry.* Energy & Fuels, 2009. **23**(4): p. 2122-2128.
11. Masliyah, J., et al., *Understanding Water-Based Bitumen Extraction from Athabasca Oil Sands.* The Canadian Journal of Chemical Engineering, 2004. **82**(4): p. 628-654.
12. Sjoblom, J., *Encyclopedic handbook of emulsion technology*2010: CRC Press.
13. Czarnecki, J., P. Tchoukov, and T. Dabros, *Possible Role of Asphaltenes in the Stabilization of Water-in-Crude Oil Emulsions.* Energy & Fuels, 2012. **26**(9): p. 5782-5786.
14. Xu, Y., et al., *Destabilization of water in bitumen emulsion by washing with water.* Petroleum science and technology, 1999. **17**(9-10): p. 1051-1070.
15. Sjöblom, J., et al., *Our current understanding of water-in-crude oil emulsions.: Recent characterization techniques and high pressure performance.* Advances in Colloid and Interface Science, 2003. **100–102**(0): p. 399-473.
16. Stanford, L.A., et al., *Compositional Characterization of Bitumen/Water Emulsion Films by Negative- and Positive-Ion Electrospray Ionization and Field*

Desorption/Ionization Fourier Transform Ion Cyclotron Resonance Mass Spectrometry. Energy & Fuels, 2007. **21**(2): p. 963-972.
17. Horváth-Szabó, G., J.H. Masliyah, and J. Czarnecki, *Phase Behavior of Sodium Naphthenates, Toluene, and Water.* Journal of Colloid and Interface Science, 2001. **242**(1): p. 247-254.
18. Horváth-Szabó, G., J. Czarnecki, and J.H. Masliyah, *Sandwich Structures at Oil–Water Interfaces under Alkaline Conditions.* Journal of Colloid and Interface Science, 2002. **253**(2): p. 427-434.
19. Czarnecki, J., K. Moran, and X. Yang, *On the "Rag Layer" and Diluted Bitumen Froth Dewatering.* The Canadian Journal of Chemical Engineering, 2007. **85**(5): p. 748-755.
20. A. Burrowes, R.M., M. Teare, C. Evans, S. Ramos, D. Rokosh, F. Rahnama, M.-A. Kirsch, L. Philp, J. Stenson, M. Yemane, J.V. Horne, J. Fong, B. Ashrafi, Greig Sankey, *Alberta's Energy Reserves and Supply/Demand Outlook*, E.R.a.C. Board, Editor 2010.
21. Vittoratos, E., G. Scott, and C. Beattie, *Cold lake cyclic steam stimulation: a multiwell process.* SPE Reservoir Engineering, 1990. **5**(1): p. 19-24.
22. Sheng, J.J., *Cyclic Steam Stimulation.* Enhanced Oil Recovery Field Case Studies, 2013: p. 389.
23. Butler, R.M., *Thermal recovery of oil and bitumen.* 1991.
24. Shen, C., *Chapter 17 - SAGD for Heavy Oil Recovery*, in *Enhanced Oil Recovery Field Case Studies*, S. James, Editor 2013, Gulf Professional Publishing: Boston. p. 413-445.
25. Nadella, N.M., *Improving Energy Efficiency in Thermal Oil Recovery Surface Facilities*, in *World Energy Congress*2010: Montreal.
26. *In situ Oil Sands Progress Presentation-Hilda Lake Pilot 8093/Orion 10103*, 2011, Shell Canada Limited.
27. *Long Lake 2011-Surface Performance Presentation*, 2012, Nexen Inc. .
28. *Surmont Oil Sands Commercial Project Approval 9426B: ERCB Annual Performance Review*, 2009, ConocoPhillips.
29. Shaw, J.M. and R. Konduru, *The behaviour of large gas bubbles at a liquid-liquid interface. Part 2: Liquid entrainment.* The Canadian Journal of Chemical Engineering, 1992. **70**(2): p. 381-384.
30. Shahrokhi, H. and J.M. Shaw, *Fine drop recovery in batch gas-agitated liquid–liquid systems.* Chemical engineering science, 2000. **55**(20): p. 4719-4735.
31. Barker, C., *Chapter 2 Origin, Composition and Properties of Petroleum*, in *Developments in Petroleum Science*, G.V.C. Erle C. Donaldson and Y. Teh Fu, Editors. 1985, Elsevier. p. 11-45.
32. Hollebone, B., *Chapter 4 - Measurement of Oil Physical Properties*, in *Oil Spill Science and Technology*, F. Mervin, Editor 2011, Gulf Professional Publishing: Boston. p. 63-86.
33. Houck, M.M., *Analytical Light Microscopy*, in *Encyclopedia of Forensic Sciences*, A.S. Editors-in-Chief: Jay and J.S. Pekka, Editors. 2013, Academic Press: Waltham. p. 609-611.

34. Bazyleva, A.B., et al., *Bitumen and Heavy Oil Rheological Properties: Reconciliation with Viscosity Measurements.* Journal of Chemical & Engineering Data, 2009. **55**(3): p. 1389-1397.
35. Richardson, S.M. and M.R. Gray, *Enhancement of residue hydroprocessing catalysts by doping with alkali metals.* Energy & Fuels, 1997. **11**(6): p. 1119-1126.
36. de Visser, S.K., et al., *Anisotropy of collagen fibre alignment in bovine cartilage: comparison of polarised light microscopy and spatially resolved diffusion-tensor measurements.* Osteoarthritis and Cartilage, 2008. **16**(6): p. 689-697.
37. Oldenbourg, R., *Chapter 10 Polarized Light Microscopy of Spindles*, in *Methods in Cell Biology*, L.R. Conly, Editor 1998, Academic Press. p. 175-208.
38. Mohammad J. Amani, M.R.G., John M. Shaw. *Volume of Mixing and Water Solubility in Water Saturated Athabasca Bitumen at High Temperature and Pressure*. in *10th International Symposium on Supercritical Fluids*. 2012. San Francisco, CA.
39. *Oil Sands Technology Roadmap:Unlucking the Potential*. 2004 [cited 2013 August 7]; Available from: http://www.acr-alberta.com/OSTR_report.pdf.
40. Keenan, J.H., et al., *Steam tables: thermodynamic properties of water including vapor, liquid, and solid phases*1969: Wiley New York.
41. Mochinaga, H., et al. *Properties of Oil sands and Bitumen in Athabasca*. in *The Canadian Society of Exploration Geologists CSPG–CSEG–CWLS Convention*. 2006.
42. Peng, M., *Thermal cracking of asphaltene by addition of hydrogen donor solvent*, in *Department of Chemical and Material Engineering*2012, University of Alberta: Edmonton.
43. Puterová, Z., et al., *Synthesis and study of new rod-like mesogens containing 2-aminothiophene unit.* Tetrahedron, 2012. **68**(39): p. 8172-8180.
44. Tong, H., et al., *Yolk spherocrystal: The structure, composition and liquid crystal template.* Journal of Structural Biology, 2008. **163**(1): p. 1-9.
45. Heinemann, C., F. Escher, and B. Conde-Petit, *Structural features of starch–lactone inclusion complexes in aqueous potato starch dispersions: the role of amylose and amylopectin.* Carbohydrate Polymers, 2003. **51**(2): p. 159-168.
46. Czarnecki, J., *Stabilization of Water in Crude Oil Emulsions. Part 2†.* Energy & Fuels, 2008. **23**(3): p. 1253-1257.
47. Czarnecki, J. and K. Moran, *On the Stabilization Mechanism of Water-in-Oil Emulsions in Petroleum Systems.* Energy & Fuels, 2005. **19**(5): p. 2074-2079.
48. Horváth-Szabó, G., J.H. Masliyah, and J. Czarnecki, *Friberg correlations in oil recovery.* Journal of dispersion science and technology, 2006. **27**(5): p. 625-633.
49. Shaw, J.M., *A Microscopic View of Oil Slick Break-up and Emulsion Formation in Breaking Waves.* Spill Science & Technology Bulletin, 2003. **8**(5–6): p. 491-501.
50. Drelich, J., et al., *The role of gas bubbles in bitumen release during oil sand digestion.* Fuel, 1995. **74**(8): p. 1150-1155.
51. Bagheri, S.R. and J.M. Shaw, *Observation of Liquid-Crystal Formation during Melting of D-(+)-Glucose.* Journal of agricultural and food chemistry, 2011. **59**(23): p. 12605-12609.
52. Wong, T.-S., et al., *Nanochromatography Driven by the Coffee Ring Effect.* Analytical Chemistry, 2011. **83**(6): p. 1871-1873.

53. Shen, X., C.-M. Ho, and T.-S. Wong, *Minimal size of coffee ring structure.* The Journal of Physical Chemistry B, 2010. **114**(16): p. 5269-5274.
54. Hunter, R.J., L.R. White, and D.Y. Chan, *Foundations of colloid science*. Vol. 1. 1987: Clarendon Press Oxford.
55. Yunker, P.J., et al., *Suppression of the coffee-ring effect by shape-dependent capillary interactions.* Nature, 2011. **476**(7360): p. 308-311.
56. Deegan, R.D., et al., *Capillary flow as the cause of ring stains from dried liquid drops.* Nature, 1997. **389**(6653): p. 827-829.
57. Hu, H. and R.G. Larson, *Analysis of the effects of Marangoni stresses on the microflow in an evaporating sessile droplet.* Langmuir, 2005. **21**(9): p. 3972-3980.
58. Parisse, F. and C. Allain, *Drying of colloidal suspension droplets: experimental study and profile renormalization.* Langmuir, 1997. **13**(14): p. 3598-3602.
59. Gorand, Y., et al., *Mechanical instability induced by the desiccation of sessile drops.* Langmuir, 2004. **20**(12): p. 5138-5140.
60. Lewis, A.T., et al., *Evaluation of the Extraction Method and Characterization of Water-Soluble Organics from Produced Water by Fourier Transform Ion Cyclotron Resonance Mass Spectrometry.* Energy & Fuels, 2013. **27**(4): p. 1846-1855.
61. Russel, W.B., *Mechanics of drying colloidal dispersions: Fluid/solid transitions, skinning, crystallization, cracking, and peeling.* AIChE Journal, 2011. **57**(6): p. 1378-1385.
62. Nguyen, V.X. and K.J. Stebe, *Patterning of Small Particles by a Surfactant-Enhanced Marangoni-Bénard Instability.* Physical Review Letters, 2002. **88**(16): p. 164501.
63. Majumder, M., et al., *Overcoming the "Coffee-Stain" Effect by Compositional Marangoni-Flow-Assisted Drop-Drying.* The Journal of Physical Chemistry B, 2012. **116**(22): p. 6536-6542.
64. Hendarto, E. and Y.B. Gianchandani, *Size sorting of floating spheres based on Marangoni forces in evaporating droplets.* Journal of Micromechanics and Microengineering, 2013. **23**(7): p. 075016.
65. Bhardwaj, R., et al., *Self-assembly of colloidal particles from evaporating droplets: role of DLVO interactions and proposition of a phase diagram.* Langmuir, 2010. **26**(11): p. 7833-7842.
66. Zhang, W., et al., *Ring formation from a drying sessile colloidal droplet.* AIP Advances, 2013. **3**(10): p. 102109.
67. Popov, Y.O., *Evaporative deposition patterns: Spatial dimensions of the deposit.* Physical Review E, 2005. **71**(3): p. 036313.
68. Sperry, P.R., et al., *Role of Water in Particle Deformation and Compaction in Latex Film Formation.* Langmuir, 1994. **10**(8): p. 2619-2628.
69. Kim, K.D., et al., *Reptation time, temperature, and cosurfactant effects on the molecular interdiffusion rate during polystyrene latex film formation.* Macromolecules, 1994. **27**(23): p. 6841-6850.
70. Mohammadi, N., A. Klein, and L.H. Sperling, *Polymer chain rupture and the fracture behavior of glassy polystyrene.* Macromolecules, 1993. **26**(5): p. 1019-1026.